2016

Coherent Beam Combining of Ultrashort Laser Pulses

Ahmad Azim
University of Central Florida

COHERENT BEAM COMBINING OF ULTRASHORT LASER PULSES

by

AHMAD AZIM

A thesis submitted for partial fulfillment of the requirements
for the Honors in the Major Program in Photonic Science & Engineering
in the College of Optics & Photonics
and in The Burnett Honors College
at the University of Central Florida
Orlando, Florida

Spring Term 2016

Thesis Chair: Dr. Lawrence Shah

ABSTRACT

Ultrashort pulsed lasers have become critical to understanding light-matter interactions in new regimes such as generation of attosecond pulses, laser filamentation, and intense relativistic processes. Development of more powerful and energetic ultrafast lasers is required for advancing these fields of study. Several petawatt class systems now exist with more in development to further scale peak power and extend the frontier of ultrafast laser technology. Another relevant solution to the scaling of energy and power of ultrashort pulses is coherent beam combining (CBC). CBC is useful for not only scaling of laser parameters but also to mitigate parasitic nonlinear processes associated with high-intensity ultrashort pulses. In addition CBC is flexible and can be implemented as part of other techniques for ultrashort pulse amplification such as optical-parametric chirped-pulse amplification (OPCPA).

In this thesis, CBC of ultrashort laser pulses is investigated based upon the method known as divided-pulse amplification (DPA). Active, passive and hybrid DPA have been achieved in a flashlamp-pumped Nd:YAG laser seeded from a Ti:sapphire mode-locked laser. Picosecond pulses at a repetition rate of 2.5 Hz were amplified and combined to record energy of 216 mJ with a combination efficiency of 80%. Engineering of the Nd:YAG amplifier chain for high-efficiency energy extraction is presented. In addition, phasing of actively divided pulses with a CW pilot laser co-propagating with the pulsed beam is also demonstrated. Analysis of multiple DPA configurations shows the viability of the method for a variety of different laser architectures including discussion of design restrictions.

ACKNOWLEDGEMENTS

First and foremost I would like to thank my thesis chair and faculty mentor Professor Lawrence Shah. Ever since he took me in to do research at the Laser Plasma Laboratory (LPL) he has given me more and more opportunities which has advanced my career as a scientist. He has given me great responsibilities although being an undergraduate at LPL which have drastically changed my life. Larry has been extremely helpful throughout the two years I have been working at LPL and has strong faith in my abilities. I am greatly honored to have him chair my committee and this thesis would not have been possible without the guidance he has given me.

I would like to greatly thank Benjamin Webb for his mentorship and guidance. The project in this thesis was led by Ben's great expertise in lasers. He not only pushed the project forward with his amazing leadership but he also took time in the process to fully explain to me everything in full detail along the way. Ben gave me the entire knowledge to write this paper but also showed me the engineering skills and techniques to strive in the laser field. I am greatly indebted to Ben and hope that I have assisted him greatly on completion of this project.

I would like to thank Professor Michael Chini for his mentorship and guidance during and after his involvement in PhaSTHEUS. During his time at LPL he made several significant contributions to the project with his incredible skills as a laser scientist. Along the way he not only taught me advanced laser concepts but gave great general advice for advancing my academic and professional career. After becoming a professor, Dr. Chini agreed to be part of my committee and also took time to discuss literature with me several times.

I would like to thank my Laser Engineering instructor and committee member Professor Peter J. Delfyett. Dr. D. is not only a very highly skilled and respected laser scientist but he is also one of the funniest people I have ever met. He has also been one of the best lecturer I have ever had during my time at UCF. Much of what he has taught us so far in Laser Engineering greatly helped my understanding of some of the concepts presented in this thesis.

I would like to thank Professor Martin Richardson. Dr. Richardson has also been supportive of me within LPL through offering me to work on PhaSTHEUS and represent LPL in a variety of settings.

I would like to thank Nathan Bodnar and the rest of the members of LPL who have helped me along the years and with our project.

Lastly I would like to thank my family, my mother and my sister for their support and understanding.

TABLE OF CONTENTS

LIST OF TABLES

LIST OF FIGURES

LIST OF ACRONYMS/ABBREVIATIONS

AOPDF	Acousto-optic programmable dispersive filter
ASE	Amplified spontaneous emission
BFC	Birefringent crystal
CBC	Coherent beam combining
CEP	Carrier-envelope phase
CEO	Carrier-envelope offset
CPA	Chirped pulse amplification
CW	Continuous wave
DFG	Difference frequency generation
DPA	Divided-pulse amplification
GD	Group delay
GDD	Group delay dispersion
GVD	Group velocity delay
GVM	Group velocity mismatch
HC	Hansch-Couillaud
HHG	High-order harmonic generation
HWP	Half wave plate
IAP	Isolated attosecond pulse
IDNRI	Intensity dependent nonlinear refractive index
LOCSET	Locking of optical coherence by single-detector electronic-frequency tagging
MI	Michaelson Interferometer
MZI	Mach-Zehnder interferometer
Nd:YAG	Neodymium doped Yttrium Aluminum Garnet
OPA	Optical parametric amplifier (or amplification)
OPCPA	Optical parametric chirped-pulse amplification
PBS	Polarizing beam splitter
PC	Pockels Cell
PID	Proportional-integral-derivative
PLL	Phase locked loop
PSD	Power spectral density
PZT	Piezoelectric transducer
QWP	Quarter wave plate
SI	Sagnac interferometer
SNR	Signal-to-noise ratio
SPM	Self-phase modulation
TFP	Thin-film polarizer
Ti:Sapphire	Titanium doped Sapphire
TOD	Third order dispersion

CHAPTER 1: INTRODUCTION

The advent of the laser led to a myriad of application in industry, military and science [1]. Ultrafast lasers, with sub-nanosecond pulse durations, have enabled direct observation and control of phenomena on extremely short time scales [2]. Significant advancements in spectroscopy, relativistic physics and nonlinear optics were made due to the development of new ultrashort pulse technology [3]. Applications requiring both high-energy and high-power sources such as laser filamentation [4], inertial confinement fusion [5] and high-order harmonic generation [6] have led to construction of several advanced laser facilities. The field of relativistic physics has been revolutionized by the emergence of terawatt and petawatt [7] class lasers.

There are but a few methods to scale the parameters of ultrashort pulses without becoming restricted by the intensity of the beam. In particular, intensity dependent nonlinear phenomena are difficult to avoid at high-energy levels. Chirped-pulse amplification (CPA) has become ubiquitous to ultrashort pulse amplification since 1985 [8]. In CPA, pulses are stretched in time, amplified, and subsequently recompressed to almost the original duration. Optical parametric chirped-pulse amplification (OPCPA) is a new variant of CPA, which also incorporates optical parametric amplifiers (OPAs). These two techniques have matured in generating high-energy, high-power few-cycle pulses. Also, OPCPA enables the generation of light in a wide range of spectral regions for a broad range of applications.

Recently, another method of amplification known as divided-pulse amplification (DPA) has enabled performance scaling of an ultrafast laser [9]. The DPA technique is also a form of coherent addition of pulses, requiring phasing of each combining element. DPA has been demonstrated in both spatial and temporal domains where pulses are split, amplified and recombined. Although DPA can be used in parallel with other laser amplification techniques, this

work demonstrates that the performance of a stand-alone DPA system provides efficient generation of Joule-level picosecond pulses with effective suppression of detrimental nonlinear effects.

The DPA technique has become an important tool in the construction of next generation ultrafast lasers. In this thesis we present work on the implementation of DPA with picosecond pulses with a flashlamp-pumped Nd:YAG laser. We demonstrate for the first time hybrid coherent combination of pulses where active and passive phasing techniques are used in a nested configuration. The following paragraphs outline the format of this thesis.

Chapter 2 introduces the fundamentals of ultrashort pulses. In addition the concept of OPCPA is explored, as it is the primary application of the high-energy picosecond laser described in this work. Chapter 3 outlines the design of our flashlamp-pumped Nd:YAG amplifier system. This includes description of the operation and architecture of the regenerative amplifier, and pulse amplification within flashlamp-pumped amplifiers is also discussed in detail. Chapter 4 presents the results of the divided-pulse amplification experiments. Concepts behind coherent beam combining, specifically on polarization-dependent combining techniques are presented. Results of active, passive and hybrid combining schemes are compared and discussed in terms of the limitations of the various methods. Chapter 5 briefly covers the implementation of active phase locking. Prerequisites for phase stabilization and the proper technology required for building feedback loops are discussed in this chapter, including results on steady-state phase locking using a Hansch-Couillaud detector. Lastly, chapter 6 describes several applications that would benefit not only from the development of DPA lasers, but coherently combined ultrafast lasers in general. These applications include laser filamentation, particle acceleration and high-order harmonic generation.

This work was done in the PhaSTHEUS laser facility at the Laser Plasma Laboratory at CREOL, the College of Optics & Photonics in the University of Central Florida. All of the work presented in this thesis was collaborative between myself, Benjamin Webb, Nathan Bodnar, Michael Chini, Lawrence Shah, and Martin Richardson. Some data and figures are soon to be published within the time in which this thesis is currently being written.

CHAPTER 2: ULTRASHORT PULSES

Ultrashort pulses have been fundamental to understanding high-intensity light-matter interactions. After many decades of improvements to mode-locking technology, direct generation of pulses as short as 5 femtoseconds is now possible and commercially available. The extremely short pulse durations enable precise temporal characterization and broad bandwidth is useful for fine resolution spectroscopic studies. Improving the parameters of ultrashort pulses will require further advances in laser development and lead to advances in many other fields of science.

2.1 Ultrafast Optics

2.1.1 Transform-Limited and Chirped Pulses

All ultrashort pulses can be characterized as either transform-limited or chirped. A transform-limited pulse is defined by the shortest pulse duration for a given spectral bandwidth since the time and frequency domain of any signal is related by the Fourier Transform [2]

$$\tilde{E}(t) = \int_{-\infty}^{\infty} \tilde{E}(\omega) e^{j\omega t} d\omega. \qquad (2.1)$$

Equivalently, the time durations can be related to the pulse bandwidth by

$$\Delta\tau \Delta\nu \geq TBP. \qquad (2.2)$$

The constant, also known as the time-bandwidth product (TBP), is associated with the pulse shape, where $\Delta\nu$ and $\Delta\tau$ are commonly measured at the full width half maximum (FWHM). For example a Gaussian pulse has a TBP of 0.441, while a secant hyperbolic pulse has a 0.315 TBP [1]. In the transform-limited case, the ultrashort pulse has a constant phase across all frequencies in the spectrum, and the strength of the electric field is at a maximum since the energy is packed over the shortest possible time duration [2]. When a pulse is not transform-limited, the instantaneous frequency becomes time dependent [2]. This means the frequency components of a

given spectrum arrive at different times, which leads to broadening of the time duration. This effect is similar to the sound of a birds chirp, hence the origin of the name. A transform-limited pulse acquires chirp by propagating through dispersive media or by nonlinear effects such as self-phase modulation (SPM), which will be explained in further details in the following sections.

In the design of a laser system, it is essential to know the peak power of the pulse at any given point to avoid damage of components. The peak power of a laser field is given by

$$P_{peak} = \frac{E}{\Delta\tau} \qquad (2.3)$$

where E is the energy of the pulse. Consequently the associated intensity of the pulse can be expressed using the peak power by

$$I = \frac{P}{A} = \frac{E}{A\Delta\tau} \qquad (2.4)$$

where A is the area of the laser beam. The intensity of a pulse will become important when discussing nonlinear phenomena and when avoiding the damage threshold of materials during amplification to high-energy.

2.1.2 Dispersion

Material dispersion, i.e. wavelength dependent index of refraction [10], is extremely important when considering ultrashort optical pulses with broad spectrum including higher order dispersion [10]. The Taylor series expansion of the spectral phase around the central frequency ω_o up to the fourth and fifth terms (equation 2.5) is appropriate for the approximation of the dispersion of pulses with femtosecond time durations.

$$\phi(\omega) = \phi(\omega_o) + \phi'(\omega - \omega_o) + \frac{1}{2}\phi''(\omega - \omega_o)^2 + \frac{1}{6}\phi'''(\omega - \omega_o)^3 + \frac{1}{24}\phi''''(\omega - \omega_0)^4 \ldots \qquad (2.5)$$

In the expansion $\phi(\omega_o)$ is a phase shift common to all frequencies in the pulse. The second term ϕ' is referred to as the group delay (GD) which accounts for the time delay in the carrier wave of the pulse caused by the dispersive medium. ϕ'', ϕ''' and ϕ'''' are the group velocity dispersion (GVD), third order dispersion (TOD) and fourth order dispersion (FOD) respectively [11]. All materials are dispersive and exhibit different amounts of dispersion for each order [12]. Dispersion management is fundamental in many optical applications for example imaging (chromatic aberration) and telecommunication (wavelength division multiplexing). Accurate precise dispersion calculations and models are required.

Dispersion management is the foundation of chirped-pulse amplification (CPA). Proper dispersion must be added to effectively stretch a transform-limited femtosecond pulse by a factor, typically ~10^3. Then the opposite amount of dispersion is required to recompress the pulse. Grating and prism pairs are commonly used [13]. Using double pass configurations grating/prism pairs can induce massive amounts of angular dispersion to stretch/compress pulses in a compact geometry illustrated by figure 1. Angular dispersion leads to temporal broadening since one end of the spectrum will lead or trail the other after reflecting or transmitting through these elements. In addition, spatial chirp is associated with mapping portions of the spectrum relative to the spatial beam profile.

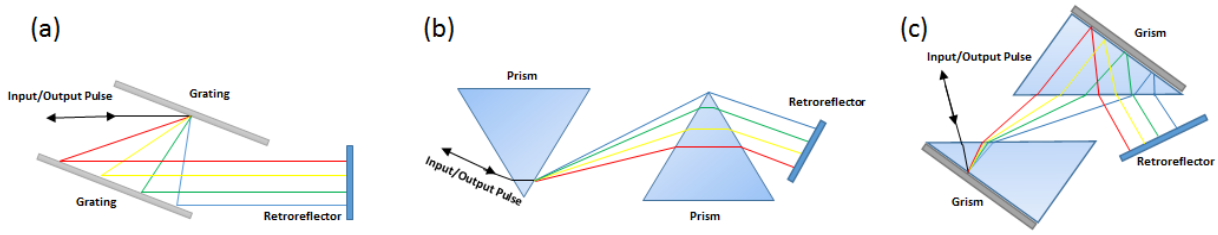

Figure 1: Several stretcher/compressor geometries: (a) Grating pair (b) Fork prism-pair (c) Grism (grating + prism) pair

Dispersion becomes more significant as ultrashort pulses approach the few-cycle optical regime. In the case of monochromatic CW light, the electric field oscillates with a single frequency, ω, and the period associated with one oscillation of the electric field as the phase goes from 0 to 2π. The coherent combination of waves with different frequencies leads to the formation of a "wave packet". The wave packet has a pulse duration defined by a slowly varying envelope encapsulating the rapidly oscillating carrier. As the pulse duration of the envelope reduces, there are a smaller number of cycles in the pulse carrier. At this point, the phase between the pulse envelope (group velocity) and the pulse carrier (phase velocity) becomes relevant (figure 2). This phase is referred to as the carrier-envelope phase (CEP) and can be determined by

$$\Delta\varphi_{CE} = \left(\frac{1}{v_p} - \frac{1}{v_g}\right)\omega_c L. \qquad (2.6)$$

In equation 2.6 v_p and v_g are the phase and group velocity of the pulse respectively, ω_c is the carrier frequency, and L is the length of the dispersive medium in which the pulse propagates. The CEP determines the peak of the electric field relative to the timing of the pulse. As the pulse approaches single-cycle time durations drifting of CEP can cause dramatic changes in the strength of the electric field within a half-cycle. Control of the CEP therefore must be ensured in order to deliver the peak of the electric field accurately for high-field processes [11]. Many methods exist for measurement and stabilization of the CEP, most notably the f-to-2f method [14]. Since ultrashort pulses can be considered as a frequency comb, the relative frequencies can be written as

$$f_n = nf_{rep} + f_{CEO} \qquad (2.7)$$

where f_n is the nth frequency component in the comb, n is an integer, f_{rep} is the repetition rate or spacing of the frequency components in the comb and f_{CEO} is the carrier-envelope offset (CEO) frequency.

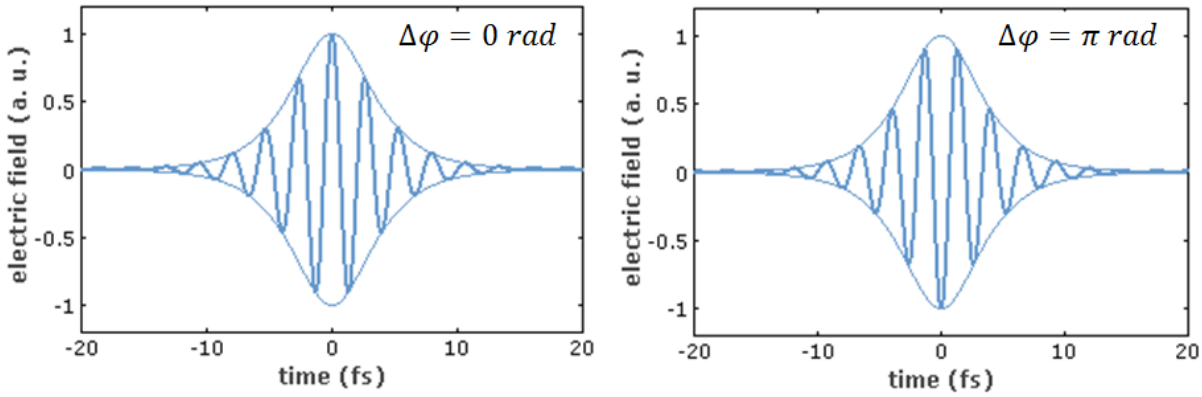

Figure 2: Left: Few-cycle pulse with a CEP of 0 radians. Right: Few-cycle pulse with a CEP π radians. From [15].

The CEO is the offset in the frequency domain due to the varying CEP of successive pulses. In order to properly observe the CEO, the oscillator repetition rate must be stabilized. In the f-to-2f method a fundamental pulse is mixed with its second harmonic to determine the f_{CEO} by the generated beat frequency. Then by using an active feedback system one can stabilize the drifts of the CEP. As the pulse propagates throughout a system another feedback loops must be implemented for the correction of both fast and slow drifts.

2.1.3 Nonlinear Optics

Nonlinear optics is intimately related with short and ultrashort laser pulses. The origins of nonlinear interactions are from the dielectric polarization $P(t)$ [3] which can be expressed as

$$P(t) = \varepsilon_0[\chi^{(1)}E(t) + \chi^{(2)}E^2(t) + \chi^{(3)}E^3(t) + \cdots]. \qquad (2.8)$$

As the electric field strength increases, so does the importance of higher order susceptibilities $\chi^{(n)}$ terms in the approximation of the material polarization. Second order $\chi^{(2)}$ and third order $\chi^{(3)}$ susceptibilities are seen in a variety of materials.

One of the main nonlinear effects that must be considered for ultrashort pulses is intensity dependent nonlinear refractive index (IDNRI) also known as the optical Kerr effect [16].

$$n(r) = n_0 + n_2 I(r) \qquad (2.9)$$

The IDNRI is the sum of linear refractive index n_0 and the nonlinear refractive index n_2 multiplied by the optical intensity. For a Gaussian beam, the spatial distribution is such that the intensity is greatest at the center of the beam, such that if an intense laser pulse is sent through a medium, the IDNRI exhibits the same spatial distribution as the beam known as a Kerr lens. This can lead to self-focusing of the beam to high intensity. For a collimated laser pulse traveling through some material, a critical peak power [2] can be defined above which self-focusing will occur

$$P_C = \frac{(0.61)^2 \pi \lambda_0^2}{n_0 n_2}. \qquad (2.10)$$

The B-integral is an expression of the nonlinear phase accumulated during propagation, shown below.

$$B = \frac{2\pi}{\lambda} \int_0^L n_2 I(r)\, dz \qquad (2.11)$$

Given that the accumulated B-integral is dependent on the spatial beam distribution, a Gaussian beam will have a higher B-integral at the beam center than the outskirts [17]. Large accumulation of the B-integral is generally detrimental and can lead to breakup of the pulse or self-focusing. In the scope of CBC, obtaining spatial coherence between two pulses is challenging in the presence of large nonlinear phase shifts. For the most part, these harmful nonlinear processes have lower threshold than optical damage in laser systems.

2.2 Ti:Sapphire Mode-Locked Lasers

First demonstrated in 1964, mode-locked lasers are a mature technology which are capable of directly generating pulses as short as 5 fs [10]. Mode-locking has been demonstrated in a variety of laser gain media with active, passive and hybrid techniques. In a mode-locked laser, many longitudinal modes of the oscillator cavity are phase locked. The large number of modes results in

constructive and destructive interference, forming a pulsed signal as a consequence of beat interference. The complex time dependent electric field in an oscillator can be expressed as

$$\tilde{E}(t) = Re\left\{\sum_p E_p e^{j2\pi(\nu_o + p\nu_{FSR})t + \theta_p}\right\} \qquad (2.12)$$

where p is the mode number, given by an integer, ν_o is the fundamental laser frequency, ν_{FSR} is the free spectral range (FSR) of the cavity and θ_p is the phase of the frequency relative to some mode. The FSR can be given by

$$\nu_{FSR} = \frac{c}{2nL} \qquad (2.13)$$

where c is the speed of light, n is the index of refraction and L is the length of the cavity. The FSR is the peak frequency spacing between two adjacent modes [2]. Therefore, these modes are mode-locked if they oscillate in phase.

Several techniques exist which can modulate these modes to lock them in phase. In the active case, acousto-optic or electro-optic modulators are placed in the oscillator cavity. These active elements can be driven in either amplitude or frequency (phase) modulation configurations to induce periodic losses in the cavity to suppress CW operation and form pulses. By properly adjusting the modulation frequency relative to the oscillator round-trip time, the modes are phase matched through the modulation process thus allowing the generation of a comb of frequencies. In passive mode-locking, saturable absorbers modulate the circulating laser pulses similar to active mode-locking but with faster modulation times than any active method. Saturable absorbers have an absorption that is dependent upon the intensity of the incident light, where higher intensities have less absorption hence the name. From the passive mode-locking technique much shorter pulses can be generated due to the ability of saturable absorbers to modulate much faster than any active element and operation at high repetition rates. A special case of passive mode-locking involves the use of the Kerr lensing which is often referred to as an artificial saturable absorber.

Kerr lensing is responsible for the reduction of the beam size dependent upon the intensity of the laser field. The oscillator can be designed such that the reduced beam size induced by the Kerr lens experiences higher gain (or less loss) such that the pulsed mode is dominant. The frequency domain equivalent of the Kerr effect also known as self-phase modulation, and this effect generates new frequency components that add to the spectral bandwidth (granted it is supported by the bandwidth of the gain medium). The dynamic processes of both self-focusing and self-phase modulation have led to the some of the shortest pulses being generated directly from a mode-locked laser. Both active and passive techniques are utilized in hybrid mode-locking of diode lasers. The hybrid method allows both the control of the circulating pulse as well as the ability to generate short pulses. Another key aspect of a mode-locked laser is dispersion control as the overall cavity dispersion must be compensated over a wide wavelength band to support ultrashort pulses. Traditionally, prism or wedge pairs incorporated into the cavity to provide adjustable dispersion. Chirped mirrors can also be utilized to compensate for higher order dispersion for broadband ultrashort pulses.

Ti:Al_2O_3, Ti:Sapphire, is a tunable laser gain medium which can emit almost octave-spanning bandwidths (a bandwidth where its highest frequency is twice or more its lowest frequency). Ti:Sapphire crystals have been used in mode-locked oscillators to achieve pulse trains with few-cycle pulse durations covering the 650 nm – 1.1 μm spectral band. Ti:Sapphire is a transition-metal solid-state laser which have phonon-assisted transitions, resulting in tunable four-level laser behavior. For our system, the near-infrared (1064 nm) band directly matches the center wavelength of Nd:YAG. We seed our Nd:YAG laser with a portion of the Ti:Sapphire spectrum so that the laser can be optically synchronized for a future OPCPA system. Various properties of Ti:Sapphire are given in table 1 which are useful for calculations.

Property	Value
Index of refraction	1.76
Fluorescent lifetime	3.2 μs
Fluorescent linewidth (FWHM)	230 nm
Peak emission wavelength	780 nm
Stimulated emission cross section (0.795 μm)	2.8×10^{-19} cm^2
Saturation fluence at 0.795 μm	$E_s = 0.9$ J/cm^2

Table 1: Tabulation of important properties of Ti:Sapphire. From [4].

In this thesis, an Idesta-QE Ti:Sapphire Kerr lens mode-locked pumped by a green (533 nm) diode laser is used as the front end shown in figure 3. The dimensions of the oscillator are 20.2''x10.5'', it has a repetition rate of 85 MHz and generates pulses with <6 fs pulse duration and 1.5 nJ pulse energy.

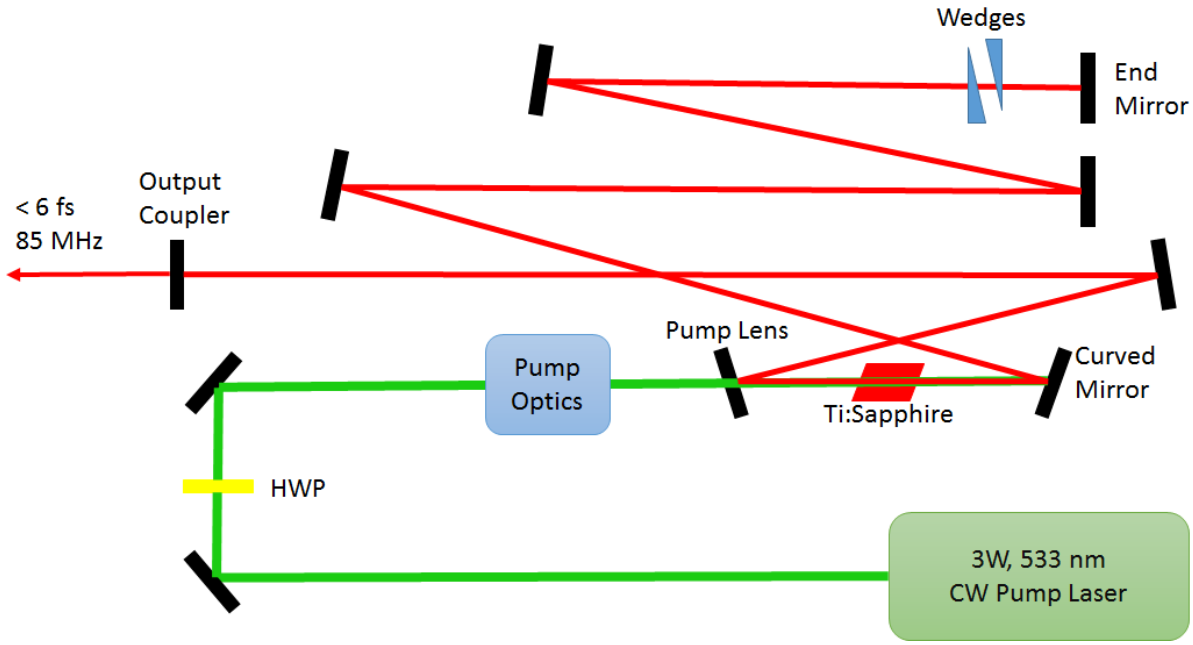

Figure 3: Ti:Sapphire mode-locked oscillator.

In the mode-locked operation of the oscillator, several adjustments must be made to the alignment of the curved mirror, pump lens and the position of the Ti:Sapphire crystal to optimize mode-

locking. Pulse formation requires several conditions to be met within the cavity simultaneously. First the pump laser must be imaged such that there is a tight beam spot inside the Ti:Sapphire crystal. The intensity in the Ti:Sapphire crystal should be high enough to generate self-phase modulation of the pulses [2]. Secondly, the dispersion must be optimized across the entire spectral band. Two intra-cavity bulk wedges are placed before the end mirror, and the position of these wedges is adjusted to fine tune the dispersion. Initiating the mode-locking by kicking the end mirror is done by changing the intensity since the focal point shifts. Pulsed operation will then be highly favorable with the Kerr lens and can be improved by the alignment of the cavity. The stability of the mode-locking is sensitive to the environmental conditions such as temperature and humidity as well as mechanical vibrations. Due to the broad bandwidth of the oscillator, it is possible to take a portion of the oscillator output at 1064 nm to seed our Nd:YAG amplifier chain so that its output can be optically synchronized to pump the OPCPA system..

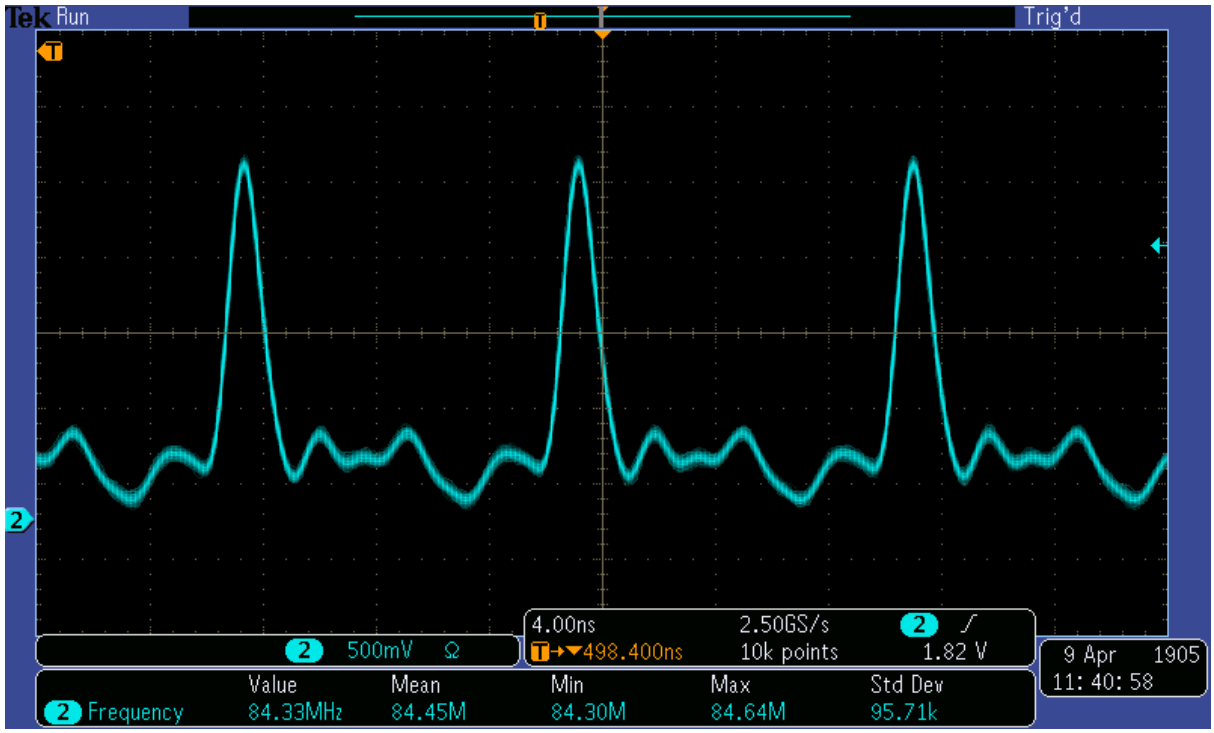

Figure 4: Screenshot of an oscilloscope trace of output of the mode-locked Ti:Sapphire oscillator with a measured repetition rate of 84.45MHz.

2.3 Optical Parametric Chirped-Pulse Amplification

In the last decade, two powerful ultrafast amplification methods, CPA and OPA, have merged together to form the method now known as OPCPA [18]. Traditionally CPA has been a more mature technology for amplifying ultrashort pulses to high-energy. However, due to gain narrowing CPA cannot support few- or single-cycle pulses. OPA is an alternative method, which supports broader bandwidth by utilizing nonlinear wave mixing to achieve gain. In OPCPA, an OPA is used rather than a laser gain medium. As an evolution of CPA, OPCPA has proven particularly well suited to the generation of high-energy single-cycle pulses in a variety of spectral regions. The following two sections provide a more detailed description of CPA and OPA.

2.3.1 Chirped-Pulse Amplification

CPA is now employed in the majority of ultrafast laser systems to avoid nonlinear phenomena that can introduce modulation in the profile of a pulse as well as to prevent damage in amplifiers [13]. The premise of CPA is to generate a pulse with very large time bandwidth product to distribute the energy of an ultrashort pulse over the longest time duration practical to reduce peak power/intensity in order to avoid nonlinear effects. Typical stretching factors from the CPA technique span from 10^3 to 10^6. In basic amplification theory, the fluence, energy per unit area of the beam, during amplification must equal or surpass the saturation fluence in the gain medium in order to efficiently extract the available stored energy [19].

$$F_s = \frac{E}{\sigma_s} \qquad (2.14)$$

In CPA, the fluence is unchanged making it possible to reach high signal fluence while minimizing nonlinearity. After amplification, the stretched pulse must be un-chirped by applying dispersion opposite to that of the pulse stretcher (figure 5) using dispersive systems similar to that

discussed in section 2.3. There are substantial losses associated with stretching and compressing stages which decrease of the over system efficiency. Furthermore, the final optics in the compressor, as well as any optics outside of the compressor, must be scaled to large apertures in order to handle the peak power and avoid damage.

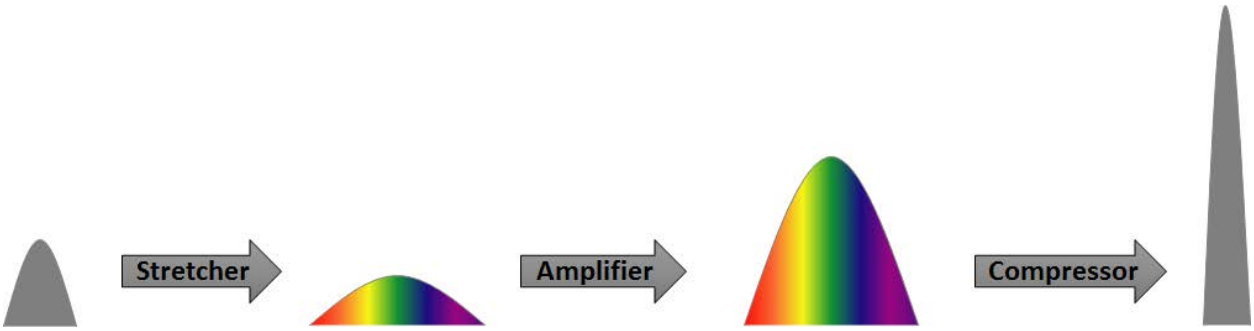

Figure 5: Flow diagram of chirped-pulse amplification

2.3.2 Optical Parametric Amplification

Whereas CPA relies on stimulated emission, optical parametric amplification (OPA) is a nonlinear process where a pump beam and a signal undergo a difference frequency generation (DFG) process [20]. DFG is based on $\chi^{(2)}$ nonlinearity where energy is transferred through wave mixing. Based on the conservation of energy, a pump photon can generate a signal and idler photon (equation 2.15) within a nonlinear crystal such as barium borate [21].

$$\hbar\omega_p = \hbar\omega_s + \hbar\omega_i \qquad (2.15)$$

However, efficient conversion also assumes momentum conservation which is achieved by phase matching the signal and pump wave vectors (equation 2.16). If the nonlinear material is birefringent, phase matching may be possible by careful alignment of the pump and seed beams relative to the crystal axis and can only be achieved over a certain bandwidth allowed by the group velocity mismatch (GVM). The gain bandwidth can be further increased by introducing a non-collinear angle (figure 6) between the two wave-vectors [22].

$$\overrightarrow{k_p} - \overrightarrow{k_s} - \overrightarrow{k_\iota} = 0 \qquad (2.16)$$

The technique's broad gain bandwidth make it extremely advantageous over other amplifier schemes which do not support few- or single-cycle pulses. Known drawbacks in other amplifier technology such as gain narrowing or high thermal deposition is avoided in OPA [23]. Therefore, this amplification technique can be used as the main amplification stage for a CPA system where a pulse can be stretched to a duration in the picosecond regime while maintaining a bandwidth which can support few-cycle pulse durations or shorter.

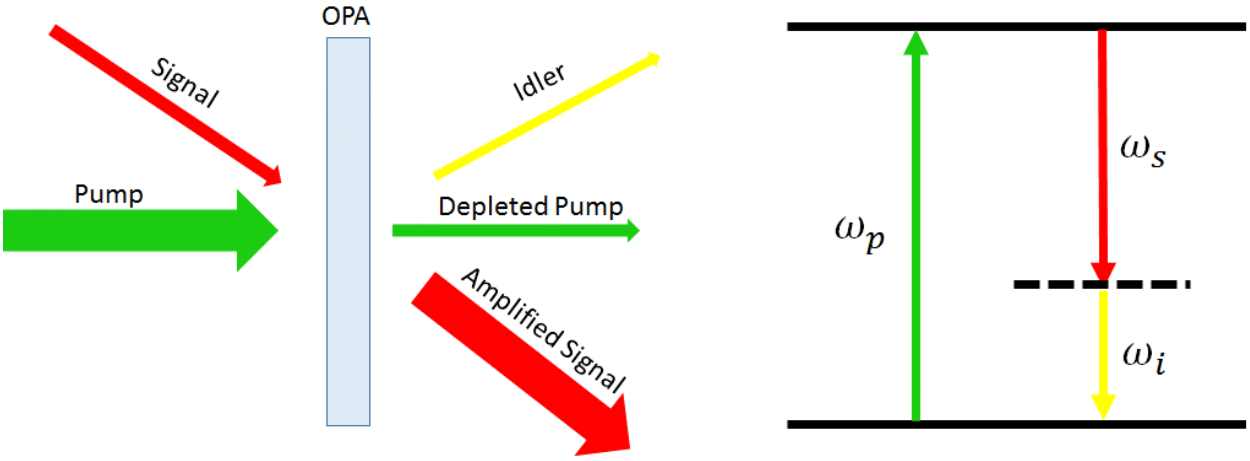

Figure 6: Left: Illustration of non-collinear OPA. Right: Virtual energy level diagram of the DFG process.

With the combination of CPA and OPA, OPCPA has been demonstrated in a wide range of average and peak powers. The performance of any OPCPA is ultimately determined by the pump laser technology used in the OPA stage [18]. The output for a few-cycle Ti:Sapphire mode-locked oscillator is split into two signals, one to seed the OPAs and the other to seed the pump for the OPA. This provides optical synchronization between the pump and signal for the OPA stage(s). In the OPA, the pump pulse duration must be slightly longer than the chirped signal pulse (typically in the picosecond range) in order to enable efficient energy transfer. This thesis focuses on the pump beam generation in the development of the PhaSTHEUS OPCPA facility, which has been

designed to produce 250 mJ qausi-single-cycle pulses with 50 TW peak power. Figure 7 shows a schematic of the general design of the OPCPA system based on two-color pumping [24].

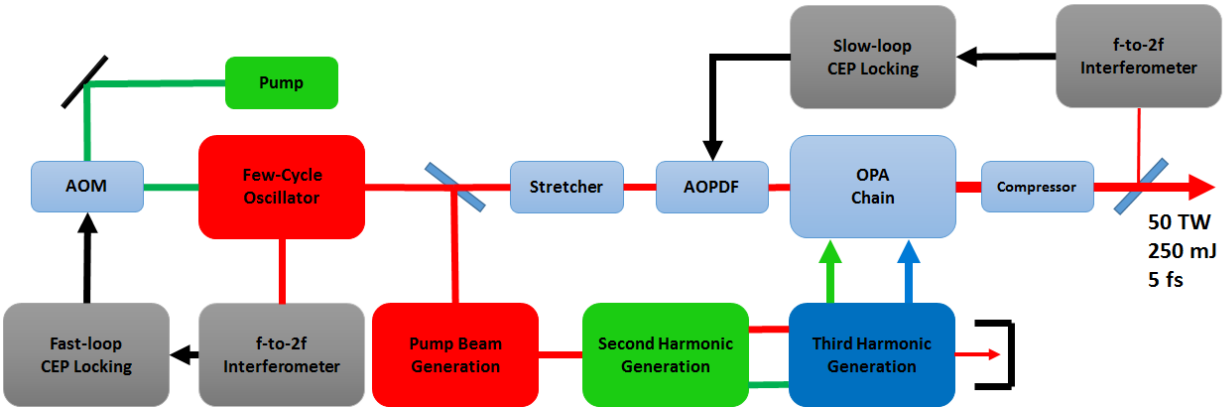

Figure 7: Schematic of proposed OPCPA system using a two-color pumping scheme and fast- and slow-loop CEP stabilization.

CHAPTER 3: ENGINEERING OF A PICOSECOND ND:YAG LASER

The pump system for the OPCPA facility incorporates Nd:YAG as the gain medium in the amplification stages. The Nd:YAG crystal rods are diode-pumped in the regenerative amplifier and flashlamp-pumped in the pre-amplifier and main beamline. Nd:YAG has many favorable features relative to DPA, as will be discussed in further details in section 3.1. This chapter covers in detail the design and engineering of our regenerative amplifier and flashlamp-pumped amplification stages for maximum output energy. As this work will show, DPA with large-aperture gain media is ideal for maximizing energy extraction while avoiding nonlinear effects while amplifying picosecond pulses. Flashlamp-pumped rod amplifiers are well established for high-energy amplification, however they do not offer ideal beam quality due to the asymmetric pump distribution within the crystal and the high thermal load. Along with the nonlinear effects, these factors determine the limit to the theoretical combination efficiency of a DPA system.

3.1 Properties of Nd:YAG

Neodymium-doped yttrium aluminum garnet or Nd:YAG is a common gain mediums for solid-state lasers. To begin with, Nd:YAG is a four-level laser medium, where there is a pump band, an upper laser state, a lower laser state and a ground state (figure 8). The laser transition occurs by stimulated emission from the upper to lower state. In a four-level system the spontaneous emission lifetime of the main transition is longer than the lifetimes of the pump to upper state and lower state to ground. This allows population inversions to be kept more efficiently therefore leading to a lower threshold pump power. The energy stored within the Nd:YAG crystal can extracted by a laser whose frequencies are supported by the gain bandwidth. Frequencies outside this bandwidth will either see no gain or can be lost to absorption.

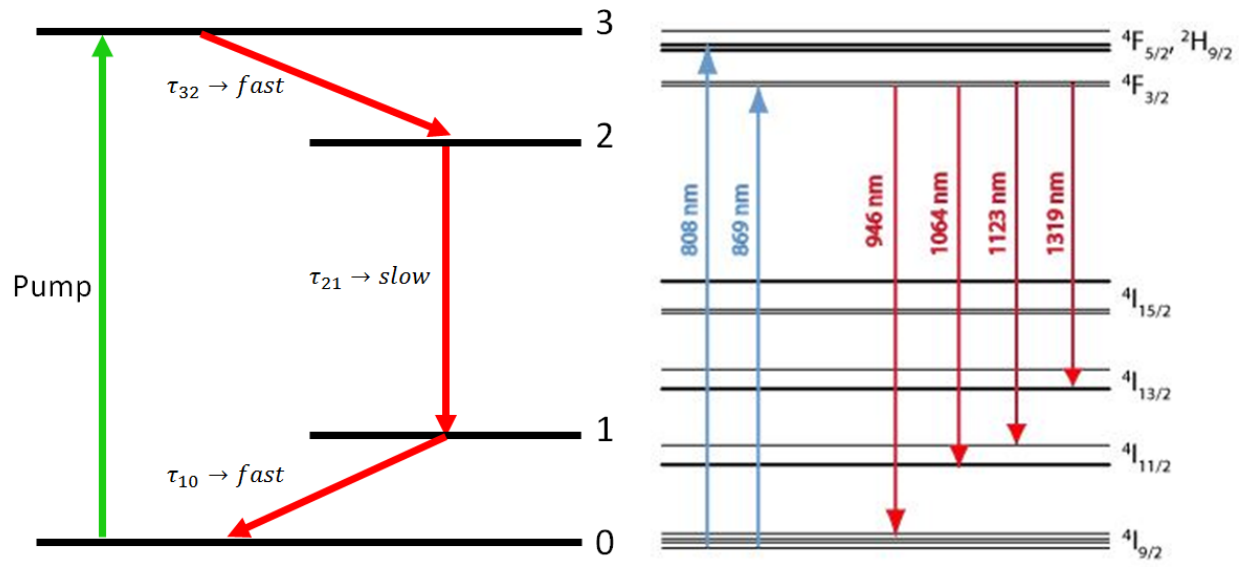

Figure 8: Left: Diagram of four-level laser. Right: Stark shifts in Nd:YAG. [25]

1064 nm is most widely utilized Nd:YAG laser wavelength, however other transitions can occur. For the $^4F_{3/2}$ level, it has been measured that only 40% of the population is associated with the 1064 nm transition. The majority of the remaining inversion is associated with 946 nm, along with emission at 1123 and 1319 nm, however all have a lower cross-section (low gain). Some of the population from the 946 nm line can replenish the 1064 nm line by phonon-assisted transition, or thermalization. This specific thermalization process can occur over time within 3-5 ns [19] and was tested using the 19 mm amplifier modules used in this system, which will be discussed in further detail in section 3.3.

This work is part of the first demonstration of DPA to maximize energy extraction in Nd:YAG amplifiers. As long as the duration of the pulse train is shorter than or equal to the fluorescence lifetime, the sum of all the pulses contributes to the saturation fluence. Table 2 list values for optical parameters of Nd:YAG which are useful for calculation for the gain characteristics.

Property	Value
Nd atoms/cm^3	1.38×10^{20}
Linewidth	120 GHz
Stimulated emission cross section (1064 nm)	2.8×10^{-19} cm^2
Fluorescence lifetime	230 μs
Photon energy (1064 nm)	1.86×10^{-19} J
Index of refraction (1064 nm)	1.82

Table 2: Tabulated values of important properties of Nd:YAG. From [19].

Pumping of Nd:YAG and other solid-state gain mediums have primarily been done using diode or flashlamp technology. Flashlamps are specially designed glass tubes housing a gas with electrodes on both ends. A high voltage introduced to the ends of the tube can trigger ionization of the gas between the electrodes, leading to an emission of incoherent broadband light. The energy of the emitted light is directly proportional to the pump voltage of the flashlamps. This broadband light is flexible to be a pump source for a variety of materials of different absorption spectrums. On the other hand a narrow bandwidth diode laser can selected to be highly resonant with the strongest absorption band of a gain medium for high conversion efficiencies. Diode pumping also allows a much more stable energy output as well as operation with higher laser repetition rates.

3.2 Diode-Pumped Nd:YAG Regenerative Amplifier

A regenerative amplifier is a laser resonator which provides high gain and helps to define the beam profile. The regenerative amplifier for these experiments has been designed (figure 9) such that the seed laser is coupled into the amplifier cavity and makes several round trips to saturate the gain medium. With a small seed energy many round trips are necessary to saturate the Nd:YAG crystal.

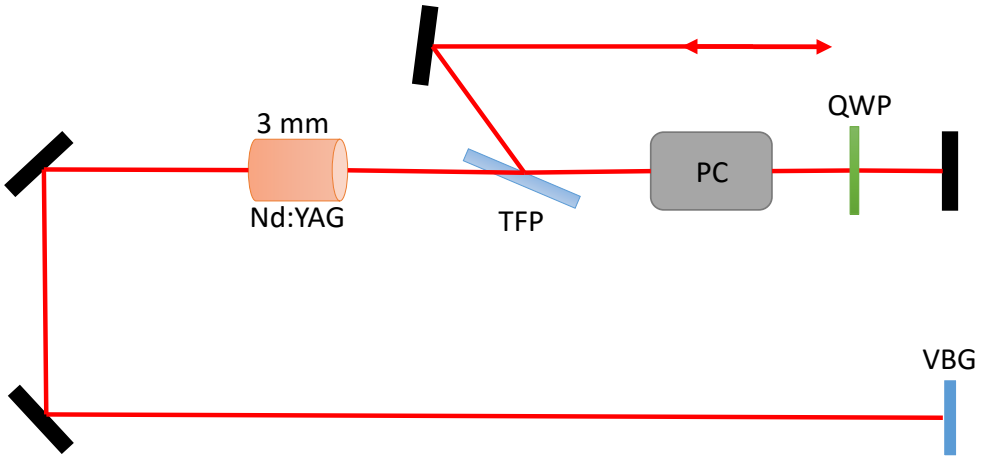

Figure 9: Schematic of regenerative amplifier. TFP: Thin-film polarizer. PC: Pockels cell. QWP: Quarter Wave Plate. VBG: Volume Bragg Graing

A Q-switch is used to enable the input coupling of the seed pulse as well as to eject the output pulse from the cavity, specifically a Pockels cell (PC) operating at the quarter wave voltage. Initially when the seed laser is injected into the resonator from the reflection off the TFP, the PC is in the off state and the double-pass through the QWP rotates the polarization of the beam so that it transmits through the TFP. Then as it is traveling towards the other end mirror, the PC is turned on to the quarter wave voltage. Note that there is a rise and fall time for the PC to reach the full quarter wave rotation. Thus the length of the regenerative amplifier cavity is chosen such that only a single pulse from the seed oscillator is trapped by the Pockels cell. With the PC held in the on position, as the laser travels through the TFP such that the return-pass through the PC acting as a QWP and the passive QWP, produce a full wave rotation such that pulse transmits through the PC and is re-amplified in the cavity for another pass. Once a sufficient number of passes have been made through the Nd:YAG amplifier to surpass the saturation fluence, the pulse is ejected out of the cavity by simply turning off the PC in the same manner it was turned on. As soon as the pulse leaves the PC for its last round trip, the PC will be turned off and as it returns to the end mirror the pulse sees a half wave voltage rather than a full wave and reflects off the TFP to counter-propagate

along its original injected path. Incident pulse energies in the nano- or micro-joule-level can be amplified up to the milli-joule regime, thus meaning regenerative amplifiers can realize a gain as high as ~10^6. In order to decouple the output from the input, a Faraday isolator can rotate the polarization of the output to make it orthogonal to the input pulse so that at a PBS they would split into different paths.

The regenerative amplifier can be operated either as Q-switched or seeded Q-switched shown in figure 10. In the Q-switched operation, no seed laser is injected into the cavity, so the gain builds up when the PC is off and stored in the cavity until the PC is turned on to its quarter wave voltage.

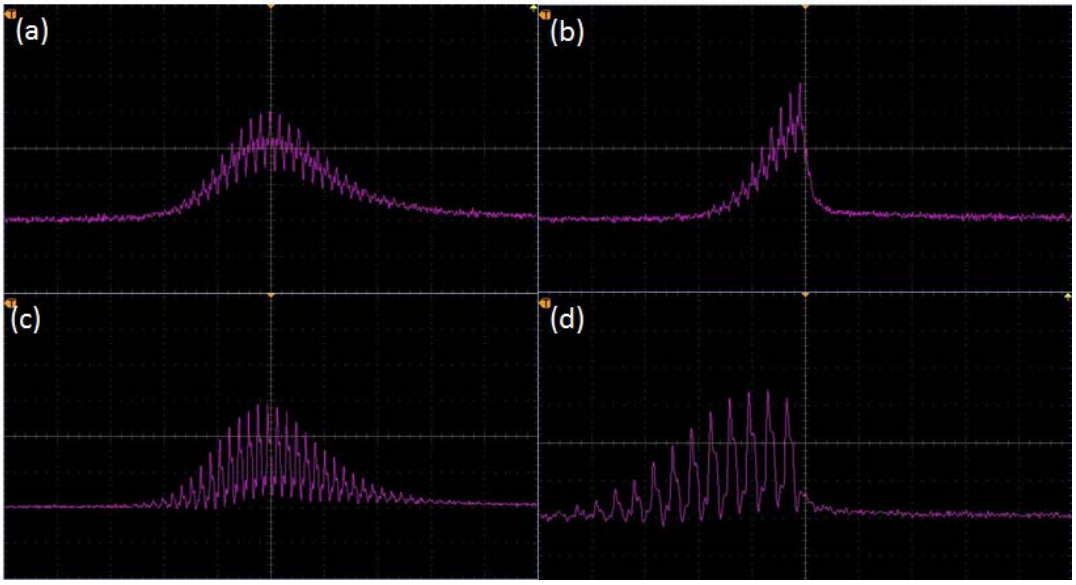

Figure 10: (a) Unseeded cavity pulse buildup. (b) Unseeded cavity pulse with Q-switching. (c) Seeded cavity pulse buildup. (d) Seeded cavity pulse with Q-switching.

A key feature in the design of this particular regenerative amplifier is the volume Bragg grating (VBG) used as one of the end mirrors of the resonator. A VBG is a dispersive element which is used in this system is used to narrow the pulse spectrum during each pass in the regenerative amplifier. With this element in place, active control of the pulse duration can be achieved in the amplifier by controlling the number of round trips the pulse makes via the PC. The PC used in the

operation of the regenerative amplifier in this system is Q-switched at a rate of 2.5 Hz, and the pulse duration when seeded is 230 ps. This becomes a quick and integrated way for tunable picosecond pulses (figure 11) which would have otherwise required grating or prism based stretchers for stretching of the Ti:Sapphire pulses. However these stretchers would only produce chirped pulses and therefore, the VBG offers the ability to create transform-limited picosecond pulses directly from a broader pulse.

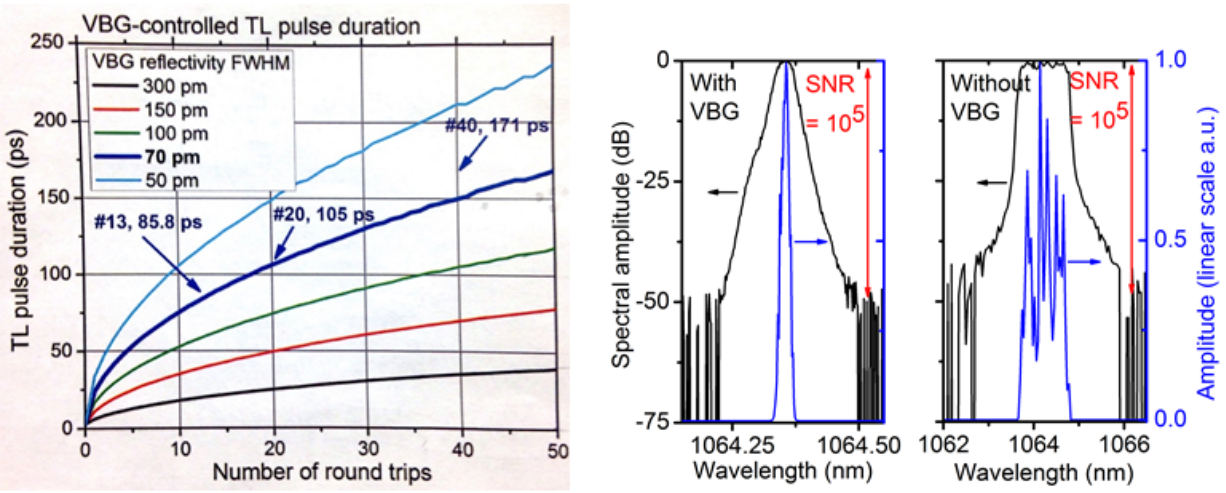

Figure 11: Left: Plot showing the transform-limited pulse duration as a function of round-trips in the regenerative amplifier. Right: Spectral amplitude plots of the resultant output pulse spectrum from the regenerative amplifier with and without the VBG.

3.3 Design of Flashlamp-Pumped Nd:YAG Amplifier Chain

After the regenerative amplifier, several flashlamp-pumped Nd:YAG amplifiers are used for energy scaling during the DPA tests done in chapter 4. The majority of amplifiers used in this work are based on flashlamp pumping. Flashlamp pumping enables relatively high-energy output, although it is less efficient than diode pumping and therefore is restricted to low repetition rate. The rods used in the modules have various diameter sizes ranging from 6 mm - 19 mm. A single 6 mm amplifier is used in a double-pass configuration since the seed from the regenerative amplifier is not high enough to saturate it with a single-pass. Then 7 mm and 10 mm rods are

arranged in series in a single-pass configuration in the experiments. After exiting the 7 mm rod and before entering the 10 mm rod, a telescope is used to increase the beam size so that the beam completely fills the aperture of the rod. 19 mm amplifier modules were used for testing the DPA technique. These rods have low small signal gain but contain a large amount of stored energy. As part of these experiments, several configurations were tested which will be discussed in chapter 4. Each amplifier unit has a separate power supply controlled from a computer as depicted in figure 12. Each of the 19 mm modules utilize four flashlamps in these modules as compared with only two flashlamps in the 6 mm, 7 mm, and 10 mm rods. Two amplifiers have the lamps clocked in a +-like configuration and two are clocked in an x-like configuration (figure 13). The arrangement of the amplifiers in two lines was chosen so that each line had one +-like and one x-like clocked module. Since the geometry of the flashlamps in the module determines the gain profile in the rod, and this setup allows for an almost uniform gain distribution for each amplifier channel. Energy extraction was tested using 10 ns pulses pre-amplified with the 7 and 10 mm rods and the energy output from each flashlamp pair is 5 J assuming a seed energy of ~500 mJ (figure 13). Therefore the total extractable energy from all four amplifiers is ~10 J.

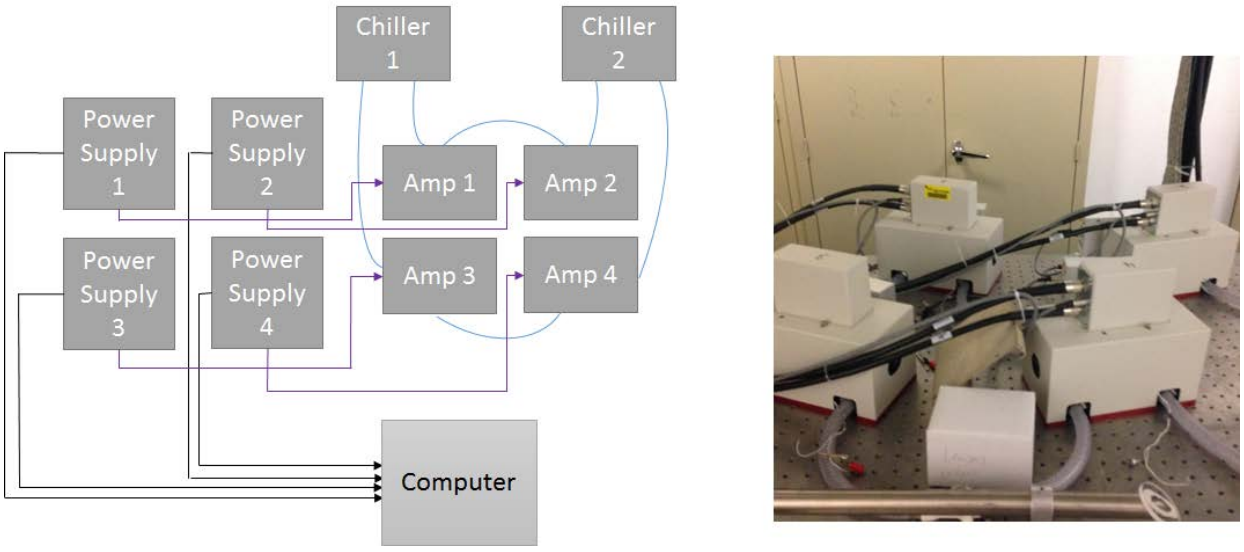

Figure 12: Schematic of 19 mm amplifier modules and supporting components.

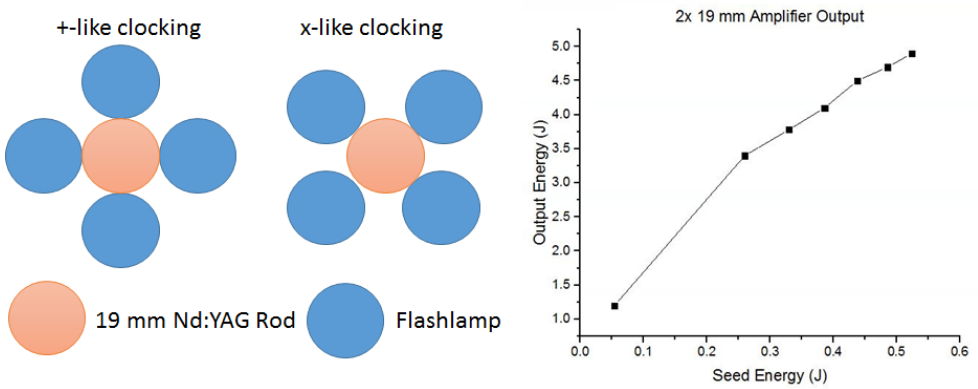

Figure 13: Left: Diagram showing the different clocking configurations of the 19 mm amplifier modules. Right: Measured gain of 2 19 mm amplifiers in line with both clockings.

In an effort to determine the best DPA configuration for compensating of thermal effects, several trials were conducted with the four 19 mm amplifiers. All 19 mm amplifiers were pumped at a max voltage of 1600V with a low seed energy of ~1 mJ. Surprisingly, no effect of thermalization was seen with four cases. The results are shown in table 3. For the DPA experiments carried out in the next chapter, the effect of thermalization was ignored due to the results obtained from this experiment. However the final system configuration was designed in order to accommodate this effect if it were to occur. From the four trials, the first case consisted of a single 10 ns pulse which has a long time duration.

Pulse Configuration	Seed Energy (mJ)	Output Energy (mJ)
10 ns	1.033	156.86
1x 230 ps	1.025	157.36
2x 230 ps (790 ns delay)	1.019	157.5
4x 230 ps (790 ns + 7 ns delay)	1.028	164.5

Table 3: Results from the thermalization experiment.

By operating the regenerative amplifier in the unseeded Q-switch operation 10 ns pulse were generated and used as the control for this experiment since the thermalization would occur less than half-way during the pulse duration. Then a single 230 ps pulse was used to seed the

amplifiers with a single pulse splitter generating two 230 picosecond pulses separated by 790 ps. In addition, the PC in the regenerative amplifier is set so as to amplify two pulses of equal amplitude separation by 7 ns. These two pulse are then sent through the pulse splitter to generate a total of four pulse in two groups separated by 790 ps and 7 ns respectively. In this experiment the variation in seed energy for all four cases were kept below 1% and the RMS stability of the pulses were around 3-4%. Thus the variations in the energy were not high enough to conclude any effects of thermalization. Several reasons may give as to why the effect was not observed. Since our input seed energy was on the order ~1 mJ, we may not have seen the effect since the amplifiers were not completely saturated, or the inversion in the main laser transition was not truly depleted.

CHAPTER 4: DIVIDED-PULSE AMPLIFICATION

Divided-pulse amplification is a method for intensity reduction of pulses for high efficiency energy extraction [26]. Relative to pulse stretching in CPA, in DPA pulses are divided into replicas prior to amplification and subsequently recombined coherently. DPA is a form of CBC, and the requirements are the same. CBC systems enable power and energy scalability relative to overall recombination efficiency and the total number of channels/replicas. Phase stabilization is required for coherent pulse recombination, either using active or passive techniques. Fundamentally, CBC is simply the coherent superposition of several wave vectors. Although simple theoretically, experimental implementation is complex with tight alignment tolerances.

Ultimately, single-aperture DPA is limited by the same damage issues as associated with long pulses and/or high average power systems. Thus spatial multiplexing is necessary for scaling towards higher energy levels. In temporal DPA, a larger amount of pulse replication would require more degrees of freedom for compensating saturation effects. In spatial DPA, the increase in the number of multiplexed channels will require much more robust phase locking.

This chapter includes discussion of basic beam combining theory and the results obtained with active, passive and hybrid DPA in both temporal and spatial domains. From these results, we have demonstrated the implementation of DPA within a flashlamp-pumped Nd:YAG laser with the use of both active and passive methods for coherent addition of up to four pulse replicas.

4.1 Coherent Beam Combination

In order to coherently combine individual beams, conditions for constructive interference must be met. Three factors must be identical in order to achieve ideal constructive interference.

First, only superposition between waves with the same frequency spectrum will produce observable interference. If superposition of many waves of different frequency occurs, the resulting amplitude modulation occurs in a beat pattern leading to temporal modulation. Secondly, all combining elements must have the same polarization state for interference to occur. Lastly, the combining elements must have identical temporal and spatial phase. Spatial coherence requires identical beam size, orientation and wave fronts. Likewise, temporal coherence assumes perfect temporal overlap.

The primary metric for CBC laser system performance is most often reported in terms of the combination efficiency in terms of the experimental output power or energy as compared to the expected theoretical value. For an overall combination efficiency one must consider the spatial η_s, temporal η_t and linear polarization η_p combining efficiencies (equation 4.1) [27].

$$\eta_{total} = \eta_s \eta_t \eta_p \qquad (4.1)$$

In this equation a simple way to calculate an efficiency η is by $E_{comb} / \sum_i E_i$ where E_{comb} is the energy of the combined beam and $\sum_i E_i$ is the sum of all powers after final amplification and before pulse re-combination.

In order to provide optimal control of temporal or spatial separation among DPA pulses, interferometers are the optical system of choice. Michaelson (MI), Mach-Zehnder (MZI), and Sagnac (SI) interferometers are all useful for DPA. These interferometers can be used both as pulse splitters and combiners and are depicted in figure 14. Amplifiers can be placed within the cavity to amplify the separate components individually. In addition, phase modulators could also be utilized in the interferometers, such as placing a piezoelectric transducer on a mirror. Alignment and stabilization of these interferometers is the most challenging issue in CBC experimentally.

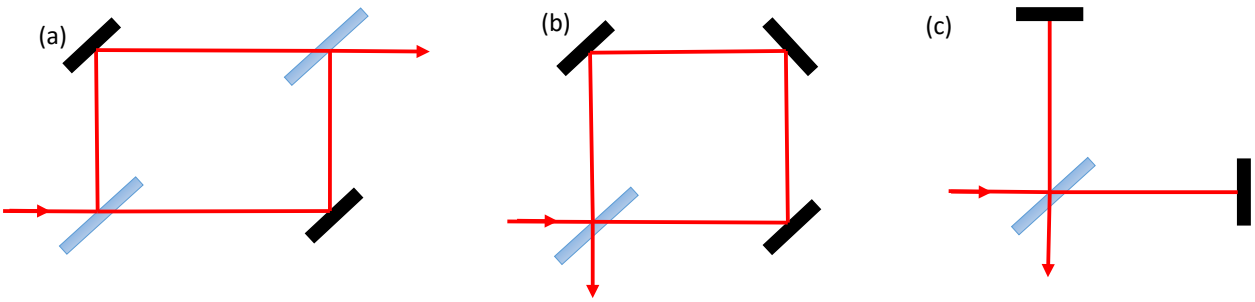

Figure 14: Various interferometer geometries. (a) Mach-Zehnder. (b) Sagnac. (c) Michaelson.

To achieve pulse splitting/combining, polarizing optics are used to resolve a pulse into two orthogonally polarized and separate pulses. Birefringent crystals (BFCs), TFPs and PBSs can be used as splitting and combining elements in the design of DPA (figure 15). If the same splitting stage is used as the both the pulse splitter and combiner, then the DPA setup is said to be passive while separate splitter/combiners systems require active stabilization [17]. Since each stage can only resolve a pulse into two separate components, 2^N pulses are produced from N splitters/combiners [9].

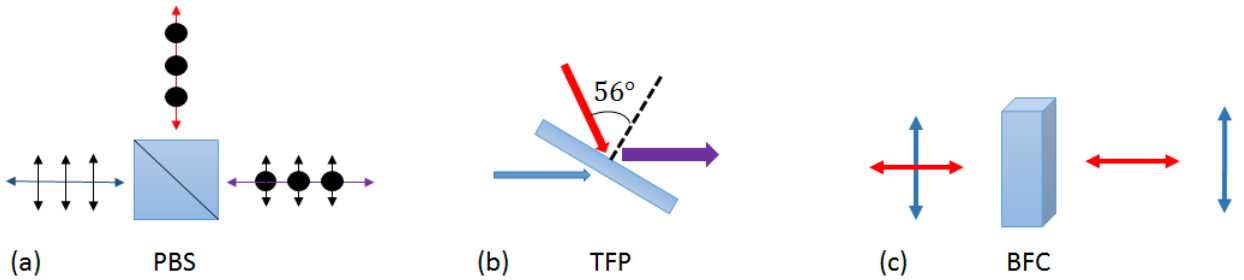

Figure 15: Different polarizing optics. (a) Polarizing beam splitter (PBS). Thin-film polarizer (TFP). (c) Birefringent crystal (BFC).

In a birefringent crystal, the ordinary and extraordinary axis have differing refractive indices [28]. Thus if an incident pulse with orthogonal polarization components propagates through the crystal with proper orientation to the crystal axes, the two polarizations travel along the two axes and exit separated in time due to the GVM. For pulse division using a sequence of birefringent crystals the required length of each successive crystal for equal separation is $L_N =$

$2^{N-1}L_N$ [26]. For high numbers of pulse replicas, crystal lengths become too large to be economically feasible for implementation.

On the other hand, polarizing beam splitters (PBSs) or thin-film polarizers (TFPs) transmit one polarization component while reflecting the other. The spatially separated p-polarized and s-polarized pulses can be recombined using a folded path, thus forming two temporally separated pulses with a time delay equal to the optical path difference. In this thesis, PBSs and TFPs with high damage threshold are used with various aperture sizes to implement the DPA technique. During the combination process, a HWP is used to rotate the combined cross-polarized pulses so that the linear polarization matches with the transmission axis of a TFP (see figure 16).

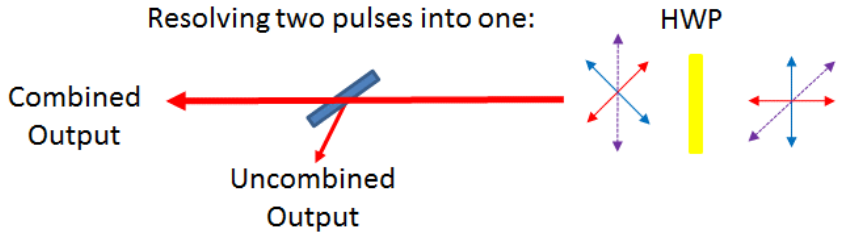

Figure 16: Coherently combining two pulses into a single polarization state using a HWP and TFP.

One of the major complications in the application of DPA is gain saturation. Since the upper state lifetime of optical amplifiers are much longer than the duration of short pulses, initial pulse replicas will have higher gain than subsequent one [19]. Thus, the pulse train must be shaped such that the first pulse to enter the amplifier has the lowest relative amplitude [29]. The orientation angle of a half wave plate (HWP) can be chosen so that one polarization component is attenuated, allowing for simple shaping before entering splitter or for adjustment after combiner. Combination efficiencies will suffer without the compensation of gain saturation due to differences in amplitude and the accumulated nonlinear phase of each pulse [30]. Scaling of DPA to larger numbers of

divided pulses is limited by the degrees of freedom required to stabilize the arms of the interferometers forming the splitters/combiners [31].

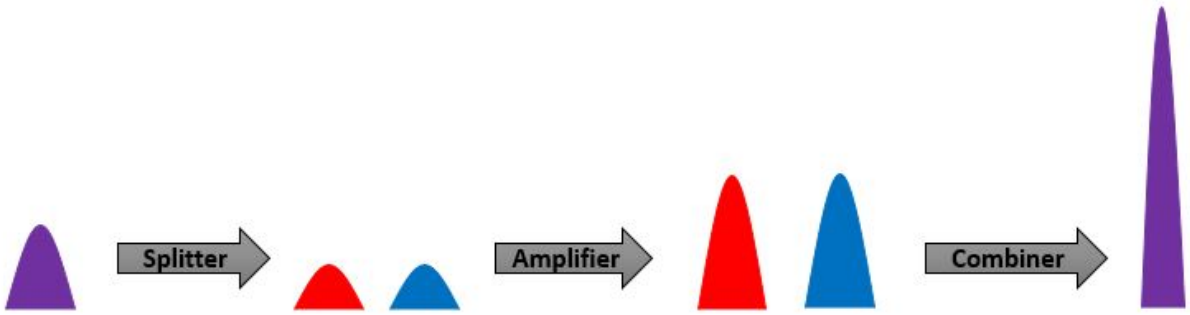

Figure 17*: Flow diagram of divided-pulse amplification.*

4.2 Active Divided-Pulse Amplification

In the initial experimental investigation of DPA using an Nd:YAG laser, active DPA was done using a simple two pulse replica setup shown in figure 18. An active DPA laser requires a separate splitting and combining stages whose optical path lengths for each replicated pulse are matched. The front end of the active DPA setup consists of the Ti:Sapphire oscillator, the regenerative amplifier and a double-pass pre-amplifier. After the 6 mm double-pass a 1064 nm CW laser was injected into the same optical path of the pulses. Since the pulses in the system have a repetition rate of 2.5 Hz, the CW laser is injected to provide a longer sampling time for fast feedback active phase stabilization. The performance of the phase locking will be discussed in further detail in chapter 5. The pulses and the CW beam were aligned to be collinear throughout the laser and they are orthogonal in polarization. The splitter and combiner were designed for low loss, large aperture and low back-reflection. Using interferometric free-space delay lines an arm of the splitter can be used to control the phase for active stabilization and the polarization in the combiner can be adjusted to be highly reflective for both paths. Back-reflection could not be compensated with the use of an isolator in a temporal pulse splitting configuration.

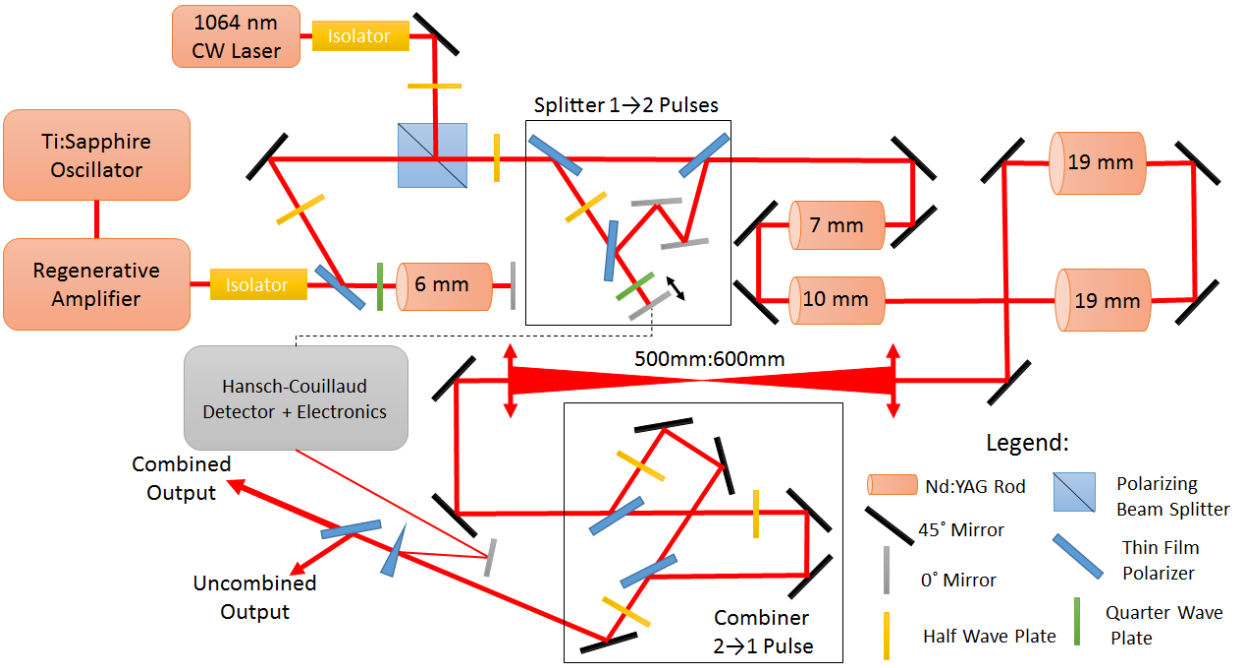

Figure 18: Laser architecture of active DPA.

The splitter is a Mach-Zenhder type interferometer which uses TFPs to resolve a cross-polarized pulse into s- and p-polarized components. The p-polarized component travels straight through and is used as the main optical path. In the reflected path of the splitter, the s-polarized pulse travels through a HWP and transmits through a TFP. Then a double-pass is made through a QWP using a 0 degree mirror mounted on a piezoelectric transducer (PZT). The mirror is also placed on a translation stage. Then as the pulse reflects off the TFP and two 0 degree mirrors, it is recombined in the same path of the p-polarized pulse. Collinear alignment is achieved using two 0 degree mirrors before the exit port of the splitter. The optical path length difference of the two arms is about 23.7 cm, which is equivalent to a time delay between the peaks of two pulses by 790 ps. This time delay is enough to resolve a 230 picosecond pulses into two replicas with orthogonal polarizations. In the 10 ns case, the two replicated pulses are almost completely overlapped with little separation.

Coalignment of the CW beam and pulses was critical to obtain the optimum combination efficiency. Although the linewidth of the pilot laser is within the gain bandwidth of Nd:YAG it has a relatively low fluence and therefore experiences negligible gain through the system. As the pulse leaves the combiner it is overlapped in space and are phase-matched to within the phase error of the feedback loop. The time delay in the s-polarization component introduced by the splitter is compensated by the combiner path length thus temporally resolving the two pulses back into a single pulse. This combined pulse contains both s- and p-polarizations with a phase error introduced in the splitter and combiner. Thus the combination efficiency was measured by how well the polarization of the pulse can be controlled to transmit through a TFP. Compensation of the amplitude differences introduced by gain saturation on the output pulse can be made by rotating the HWP after the combining TFP. The phase locking system described in chapter 5 is used to suppress the phase error due to the separate path lengths which the pulses take. Figure 19 shows the output beam profiles of both the combined and rejected outputs (the transmitted and reflected arms of the analyzing TFP, respectively). They represent the phase-matched and non-phase-matched parts of the pulse replicas. In the beam profile of the rejected output, it can be seen that the wings and center of the beam were not coherently combined. This is due to the amplification asymmetry between the two pulse replicas, leading to different accumulation of B-integral in these regions. Since the flashlamps in the 7 and 10 mm amplifier modules are placed at the sides of the Nd:YAG rod, the pump absorption is much stronger in these two sides of the rod than the other portions. From a comparison of the combination efficiency of 10 ns and 230 ps pulses (figure 20) it can be seen how the B-integral degrades the performance of the system towards higher energies. The reason for a higher efficiency in the picosecond pulses at low energy can be attributed to the 3% rms energy fluctuation of the laser.

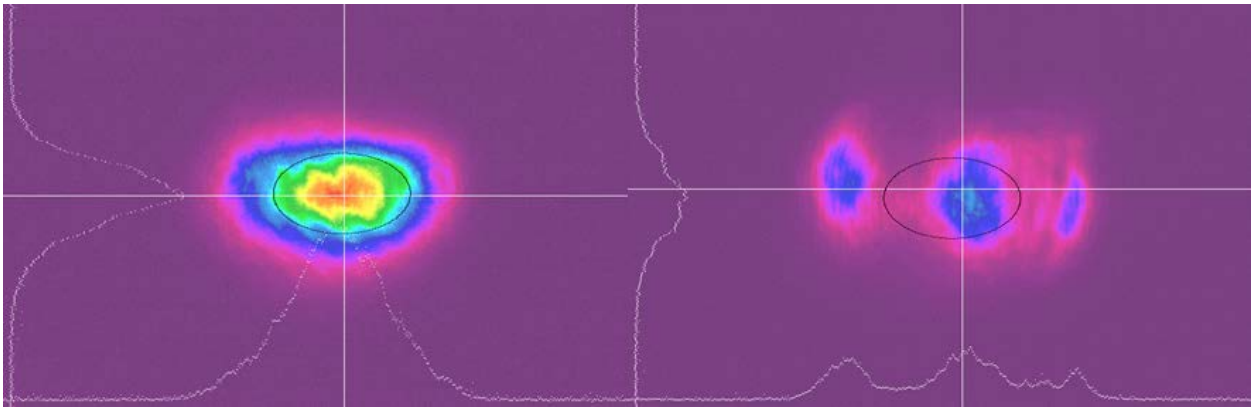

Figure 19: Left: Beam profile of combined output. Right: Beam profile of rejected output.

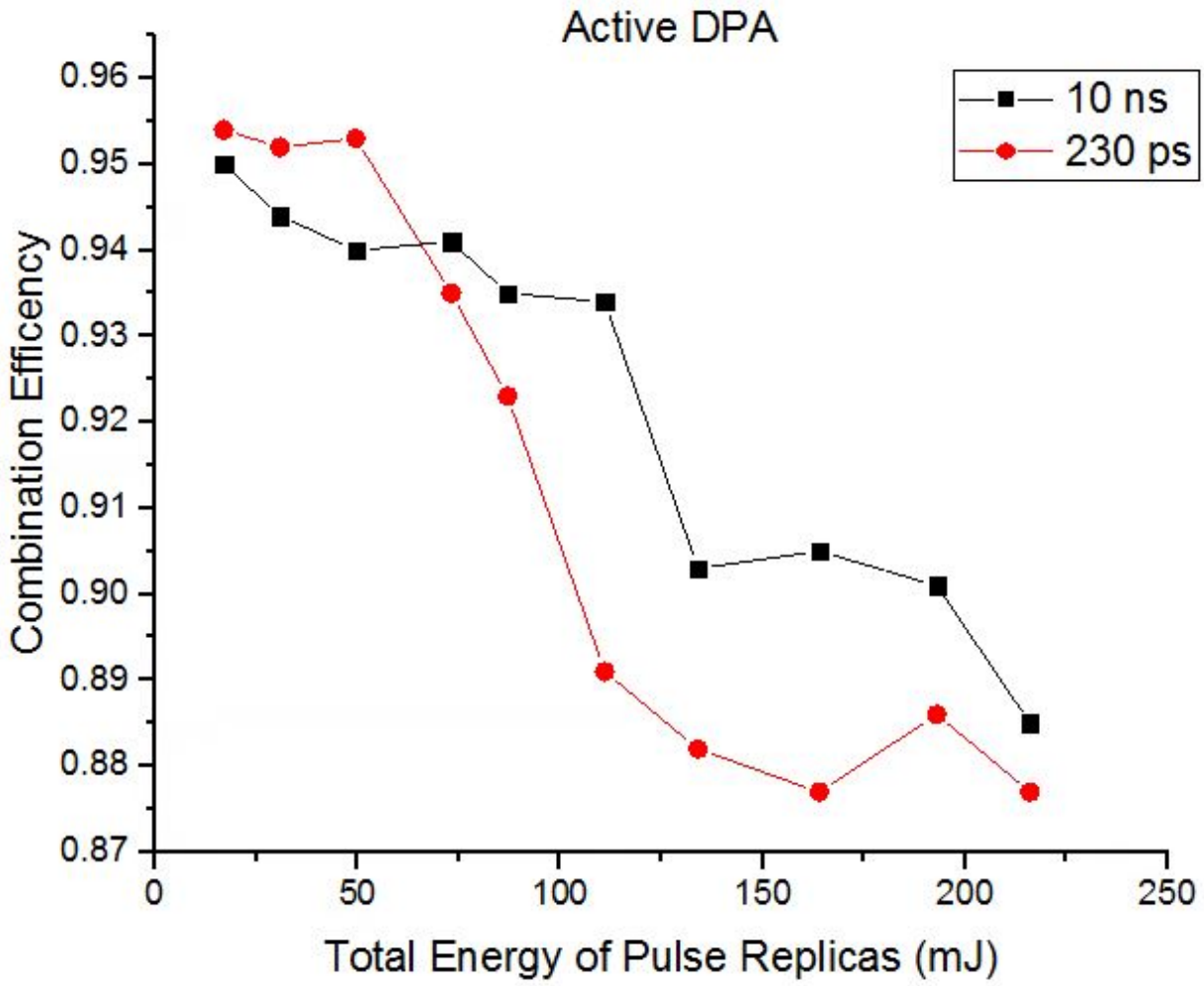

Figure 20: Combination Efficiency of the active DPA experiment as a function of the cross-polarized pulse energy.

Using an oscilloscope, a temporal tracing of the picosecond pulses before and after the combiner was taken. Figure 21 shows the 790 ps delay between the two pulses and the combined output of the output pulse. The oscilloscope does not resolve the pulse entirely since its bandwidth is < 230 ps resolution.

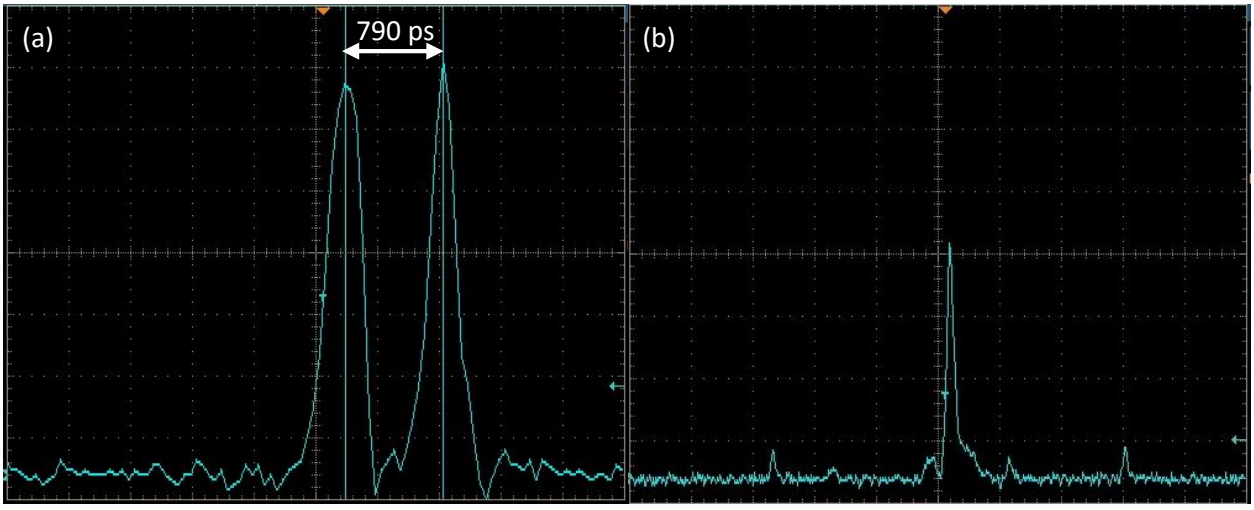

Figure 21: (a) Trace of the picosecond pulses before the combiner with a separation of 790 ps. (b) Trace of the pulse at the combiner output.

4.3 Passive Divided-Pulse Amplification

A SI was built after the amplifier chain of the active DPA configuration in the previous section. Four 19 mm amplifiers were arranged in an interferometer as depicted in figure 22. The splitter was adjusted to only have p-polarized transmission. The input pulse in the passive Sagnac-type splitter/combiner had its polarization rotated such that the electric field intensity was split 50:50 between s- and p-polarizations. Thus after the beam splitter two pulses, one reflected and one transmitted, counter-propagate through the interferometer and meet back at the PBS at the same instant with almost the same phase. This common phase shift experienced by the pulses is due to the common optical path shared by the s- and p-polarized pulses. Thus the interferometer is passively stabilized which does not require an active phase stabilization scheme. This makes the

passive DPA approach much simpler both in alignment and phasing of the pulses. However, the maximum combined energy is inherently limited by gain saturation and the damage threshold of the splitting/combining polarizing optic.

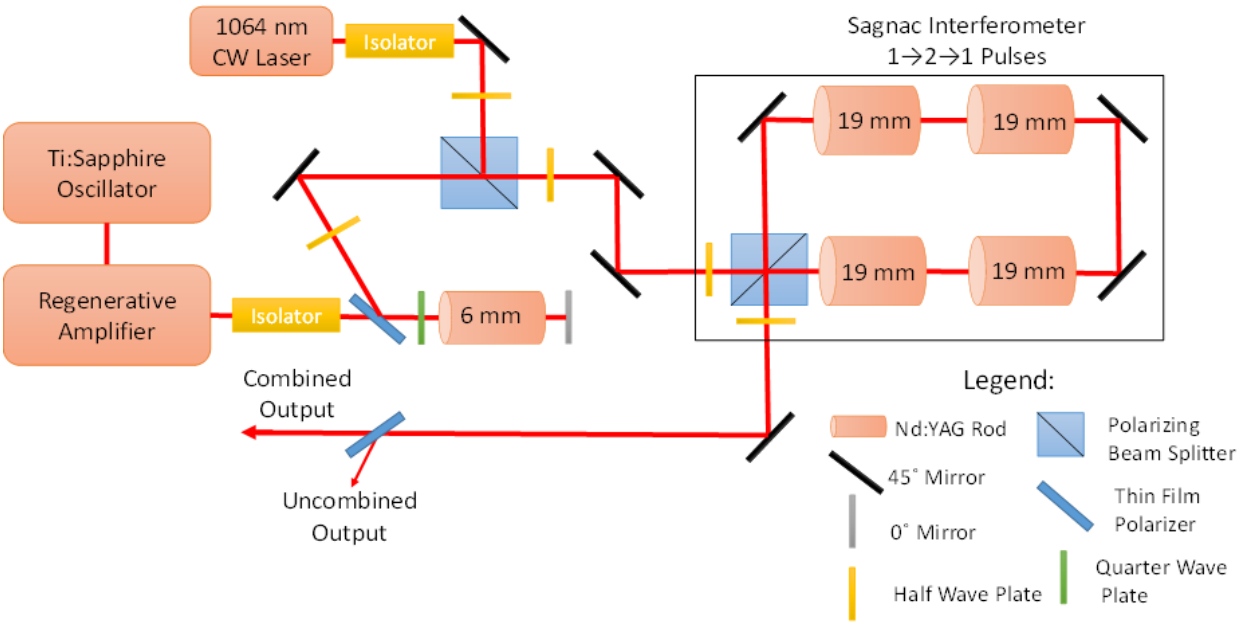

Figure 22: Laser architecture of passive DPA.

In an experimental study of the SI, a case where 10 ns pulses were seeded with none of the amplifiers on, and cases using 230 ps pulses with 0, 1, 2 and 4 amplifiers pumped. As the number of pumped amplifiers increased, the alignment of the SI changes due to the increase of the total thermal loads of the rods. The heat created by an increased pump voltage will introduce slight expansion of the crystal as well as a slight variation of the refractive index. The alignment had to be adjusted several times while taking measurements of the combination efficiency at various energies. Figure 23 shows the output beam profile of SI looking after an analyzing polarizer. The left figure is the coherently combined beam while the right figure is the rejected beam profile. The energy of this beam profile is at 150 mJ, which is almost at the maximum pulse energy before damage (~185 mJ) of the PBS in the SI. The combination efficiency was plotted in figure 24, as a function of energy of the cross-polarized pulses before the analyzing TFP.

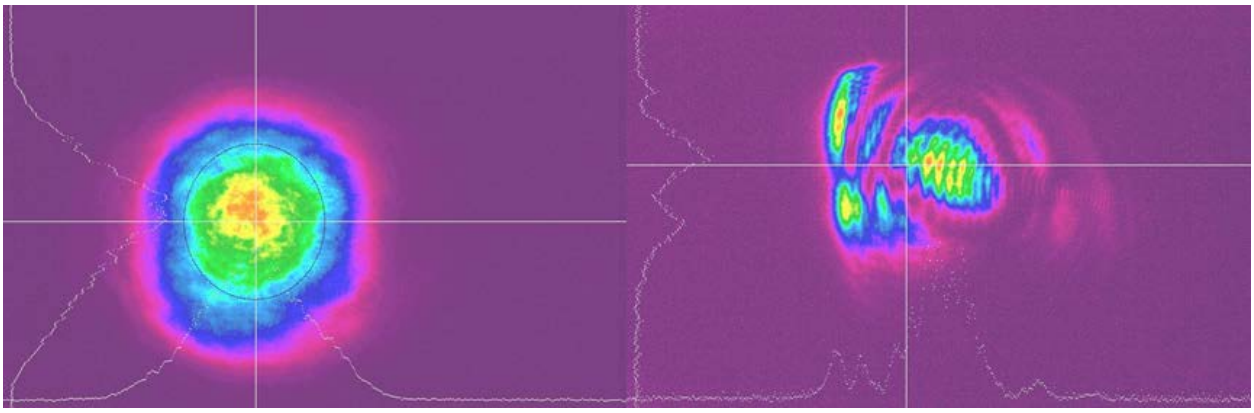

Figure 23: Left: Beam profile of combined output at a total pulse energy of 150 mJ. Right: Rejected output beam profile.

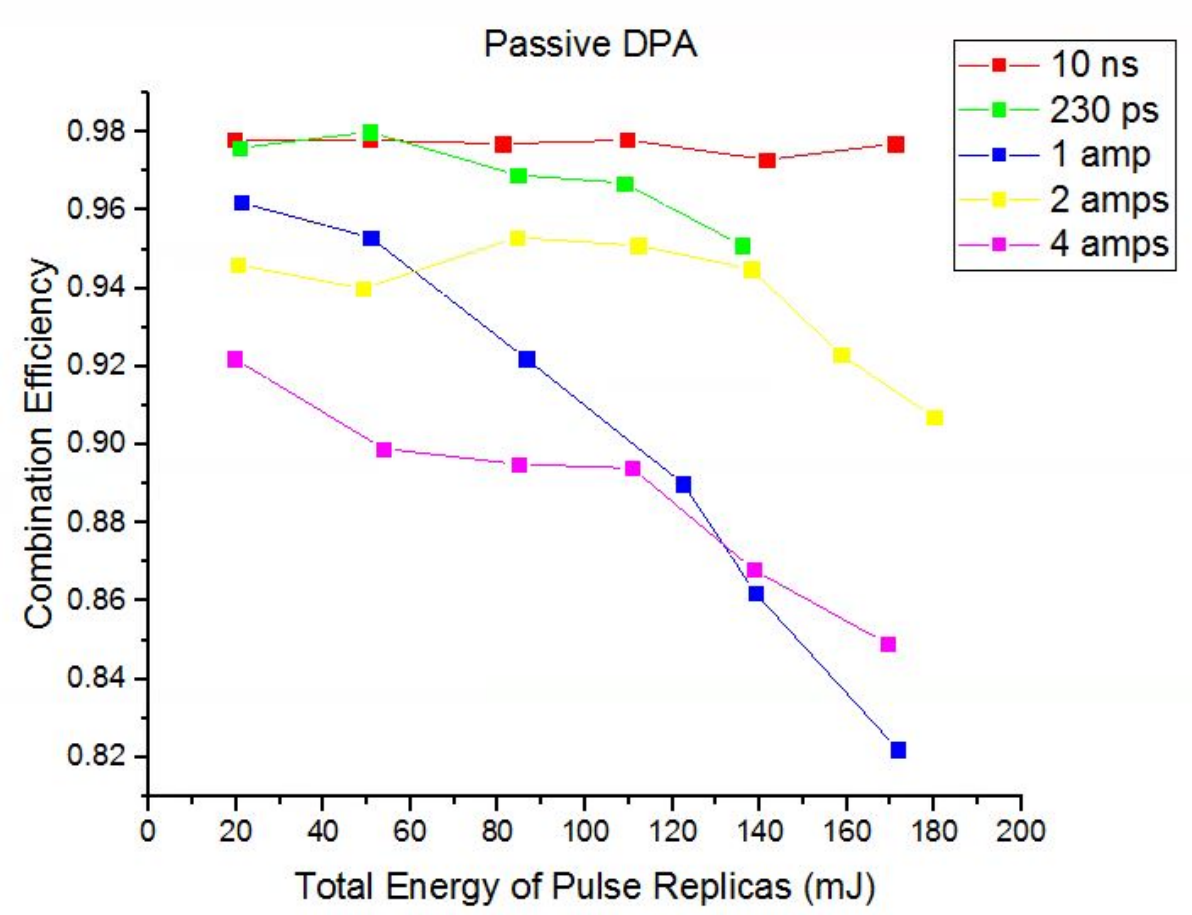

Figure 24: Combination efficiency of passive DPA versus the total energy of pulse replicas before the analyzing TFP.

Other designs for the SI can be considered for two cases. One that involves the use of a birefringent amplifier which only allows gain in one polarization component and the other involves

amplifying using circular polarization to reduce the B-integral. Figure 25 shows the configuration of two commonly used SI found in literature [16,23].

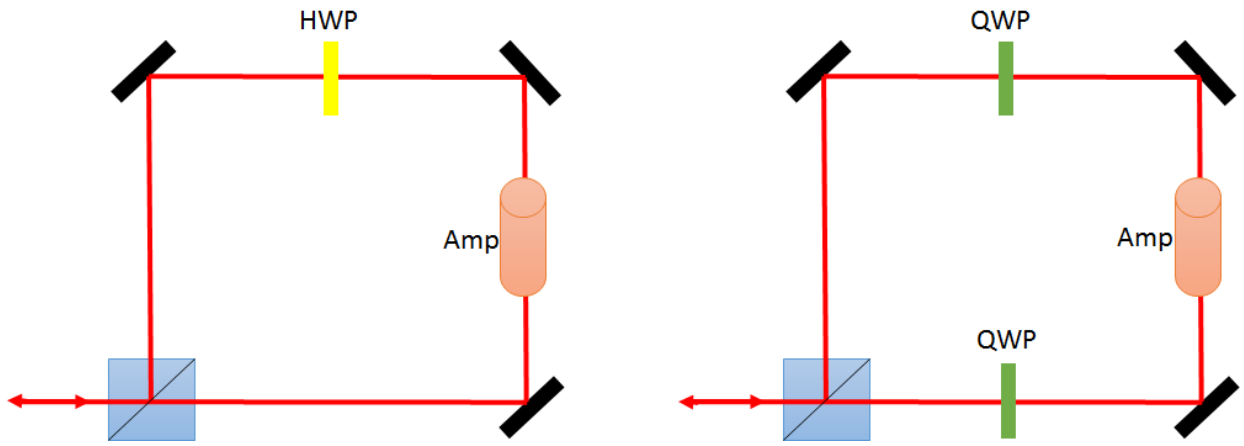

Figure 25: Left: SI setup for a birefringent amplifier. Right: SI setup for circular polarization.

For the first case, a HWP is used to rotate the replicated pulses polarization which would be orthogonal to the axis of a birefringent amplifier. Thus the incident pulses in the amplifiers will both be able to extract energy. It is known [33] that the Kerr-nonlinearity is lower for circular polarization. This can be easily implemented using the SI as shown in figure 25 (right) by placing QWPs in front of each arm of the PBS. If the amplifiers are placed in between the two QWPs each pulse will be amplified with a circular polarization and returned at the PBS with a linear polarization rotated by a half wave. In both cases the output of the SI will travel in the direction opposite to the input pulses, but along the same axis. Thus, a Faraday isolator is required to separate the output from the input. These passive combining interferometers can be scaled to a larger number of pulse replicas by cascading these two configurations. However the wave plates in the interferometers can't be tuned for compensation of the gain saturation effects at high energy. Instead, with the use of actively divided pulses they can be used effectively as a booster amplifier at a limited energy output dependent on the damage threshold of the combining port. The use of

both active and passive DPA techniques can therefore lead to an efficient and compact method of combining multiple pulse replicas requiring less active phase stabilization.

4.4 Hybrid Divided-Pulse Amplification

In a proof of principle experiment nested active and passive DPA, also known as hybrid DPA, was implemented. In this configuration depicted in figure 26, a SI was placed between the splitter and combiner in the active DPA setup. With the two pulses replicated from the splitter, a HWP before the SI is used to rotate the polarizations of replicas to split evenly 50:50 thus having a total of four replicas traverse the interferometer. Two s-polarized and two p-polarized pulses counter-propagate within the SI and extract energy from the two 19 mm amplifiers. The four pulses recombine back into two pulses at PBS in the same manner with the two pulse passive DPA experiment. The HWP at the output rotates the polarizations of the two pulse replicas back to having one pulse completely p-polarized while the other completely s-polarized so that the combiner can combine them back into a single pulse similar to the active DPA setup. In this configuration we were able to split and recombine up to four pulse replicas by phase control of only one pulse replica. In addition an almost ideal combination efficiency was accomplished for combining 4 pulses to 2 using the SI. One of the drawbacks for this design for further energy scaling is the damage threshold and back-reflection of the PBS in the SI. A back-reflection at an energy of 171 mJ after the SI was measured to be 40 mJ at the PBS before the splitter. The back-reflection reached this energy since the gain of the 7 and 10 mm pre-amplifiers are high, and thus the back-reflections can become parasitic to the system and even high enough to leak through the Faraday isolator after the regenerative amplifier. In the experiment carried out using the hybrid setup, the max energy reached after the polarizer of the SI was 309 mJ. This energy is the sum of the two recombined pulse replicas both with energies ~150 mJ assuming a 50:50 split and equal

gains seen during amplification. Any further energy would have created damage in the PBS. Sending these pulses to the output of the combiner creates a system loss due to the transmission contrasts of several optical components. The total transmission of the relay tube and combiner was measured to be 88%, which thus reduces the energy of the overlapped pulses to 271.92 mJ. After combining the pulses with a combination efficiency of 80%, we obtained a maximum combined output of 216 mJ.

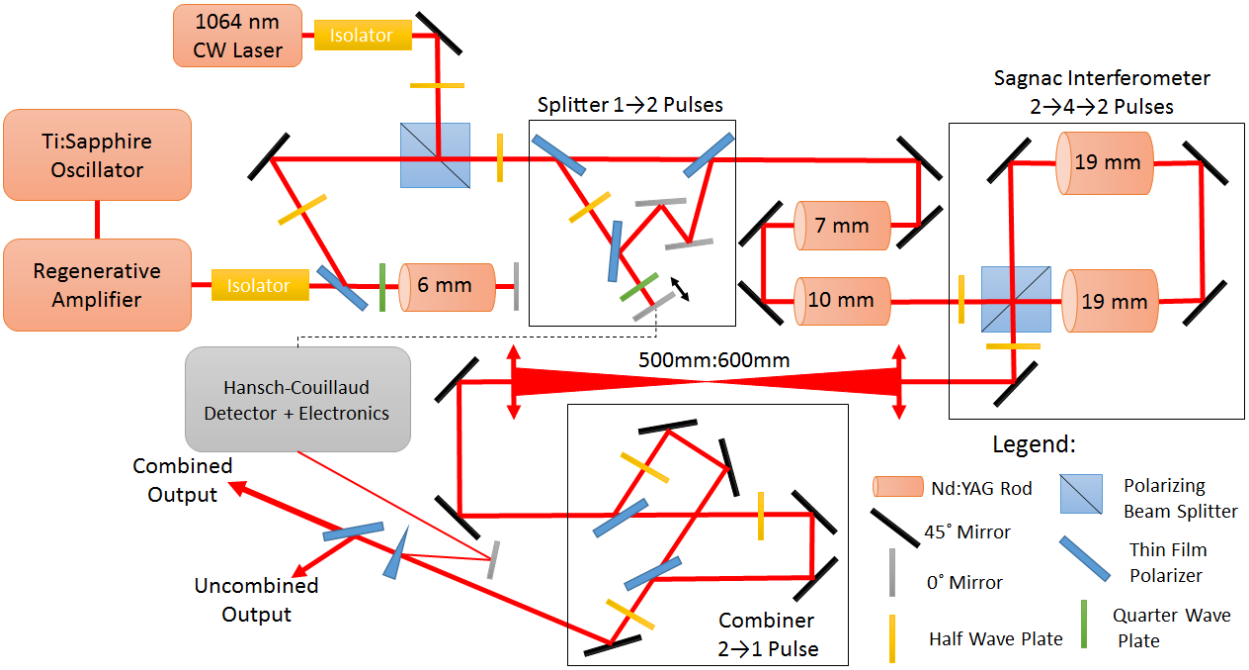

Figure 26: Laser architecture of hybrid DPA.

The beam profiles in figure 27 show the combined and rejected beam profiles after the analyzing TFP. Notice, similar to the active case, a large amount of rejection of the wings and center of the beam. This is mainly due to the pumping of the Nd:YAG rods, which see more inversion in the sides of the crystal since in most of our modules the flashlamps are placed on the sides. In addition the center of the rod sees the least inversion since much of the radiation from the lamps are absorbed more radially outwards from the center.

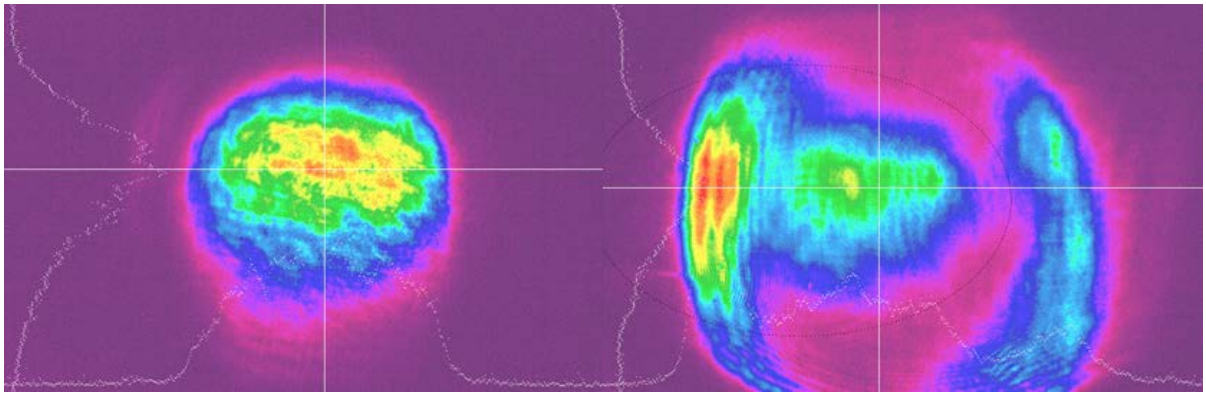

Figure 27: Left: Beam profile of the hybrid combined output at an energy of 216 mJ. Right: Beam profile or hybrid rejected output.

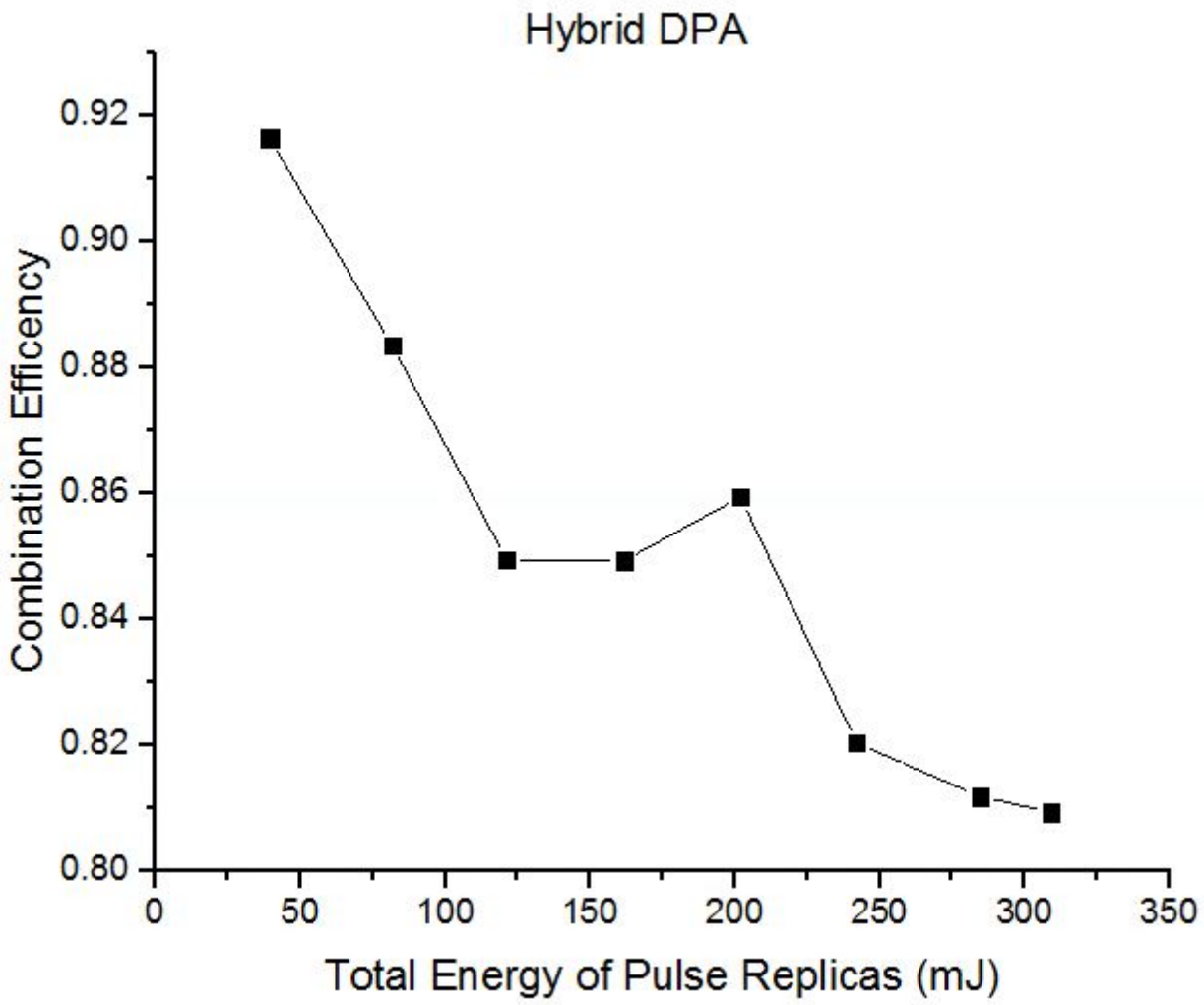

Figure 28: Hybrid DPA combination efficiency as a function of total energy of pulse replicas before the analyzing TFP.

The combination efficiency of the hybrid system plotted in figure 28 was measured as the product of the passive and active stages by analyzing after the SI and after the combiner. The energy transmission ratio of the optics from the SI to the combiner was 88% which was also included in the calculation of the combination efficiency. It is important to note that the amplifiers in the SI were not completely saturated and could have produced a higher energy output. However the system was limited by the damage threshold of the PBS in the SI which acts as the input/output port. In addition, the obtained combination efficiency for 4 pulse replicas using active phase stabilization on control of only one pulse is very comparable to the active combination of only two pulses. The hybrid scheme is therefore effective for use in a variety of DPA configurations.

Looking at the temporal contrast (Figure 29) of the combined output of the hybrid configuration we see a large accumulation of satellite pulses. The origins of these satellite pulses can determined by the distances from the main pulse. The two outer pulses which were about ~4 ns apart from the peak of the main pulse were determined to be originating from the PC in the regenerative amplifier. The closely spaced pulses around the main pulse are reflections coming off the PBS in the SI or the two-pulse combiner. Cleaning up these satellite pulses will be possible with SHG since they will not be strong enough to initiate nonlinearity.

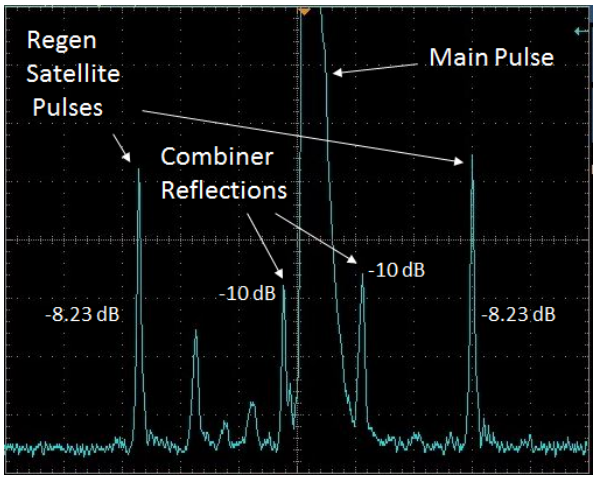

Figure 29: Temporal contrast of the hybrid DPA combined output.

4.5 Final System Design for 8 Pulse Amplification

The final system design is designed to amplify 8 pulse replicas to an energy ~10 J in order to fully extract the maximum extractable energy of the amplifiers using picosecond pulses. The front end of the final system is a temporal 4 pulse splitter and pre-amplifier shown in figure 30.

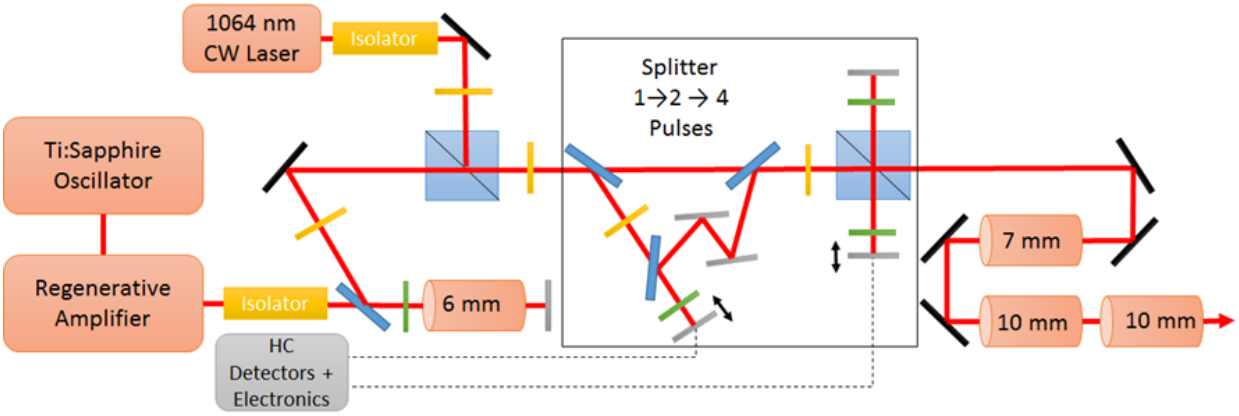

Figure 30: Front end for an 8 pulse DPA laser consisting of a 4 pulse splitter and pre-amplifiers.

After obtaining a very poor combination efficiency (~50% which is almost the theoretical minimum) from using a two-channel configuration, another approach needed to be taken. Therefore a hybrid 8 pulse spatial DPA stage was designed for efficient phasing of the pulse replicas (figure 31). When pumping the amplifiers a voltage of 1600V, the flashing of the lamps becomes very noisy. Therefore trying to actively stabilize two channels with highly fluctuating noise differences introduces too large of a phase difference for our phase locking system to compensate. In the passive case, four amplifiers could be pumped and a decent efficiency was obtained (~85%). In the passive case, the common path length which the pulses took allowed the recombination to take place without any active phasing. Thus, this final design incorporates a common path length during the amplification such that the almost the same phase shifts introduced by the flashlamp-pumping would be seen by every pulse replica to ensure effective phase locking. In addition isolators can be used to prevent high energy back reflections to the front end.

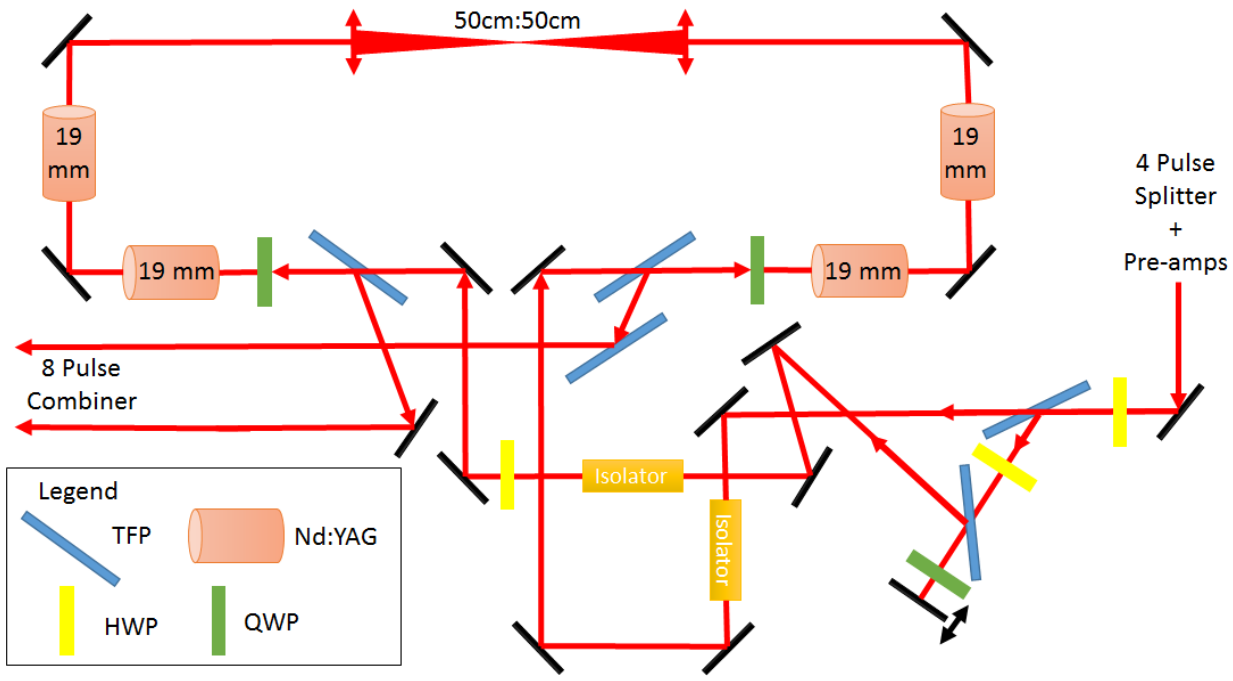

Figure 31: Design of 8 pulse hybrid-type DPA using single-channel amplification line. TFP: Thin-film polarizer. QWP: Quarter wave plate. HWP: Half wave plate.

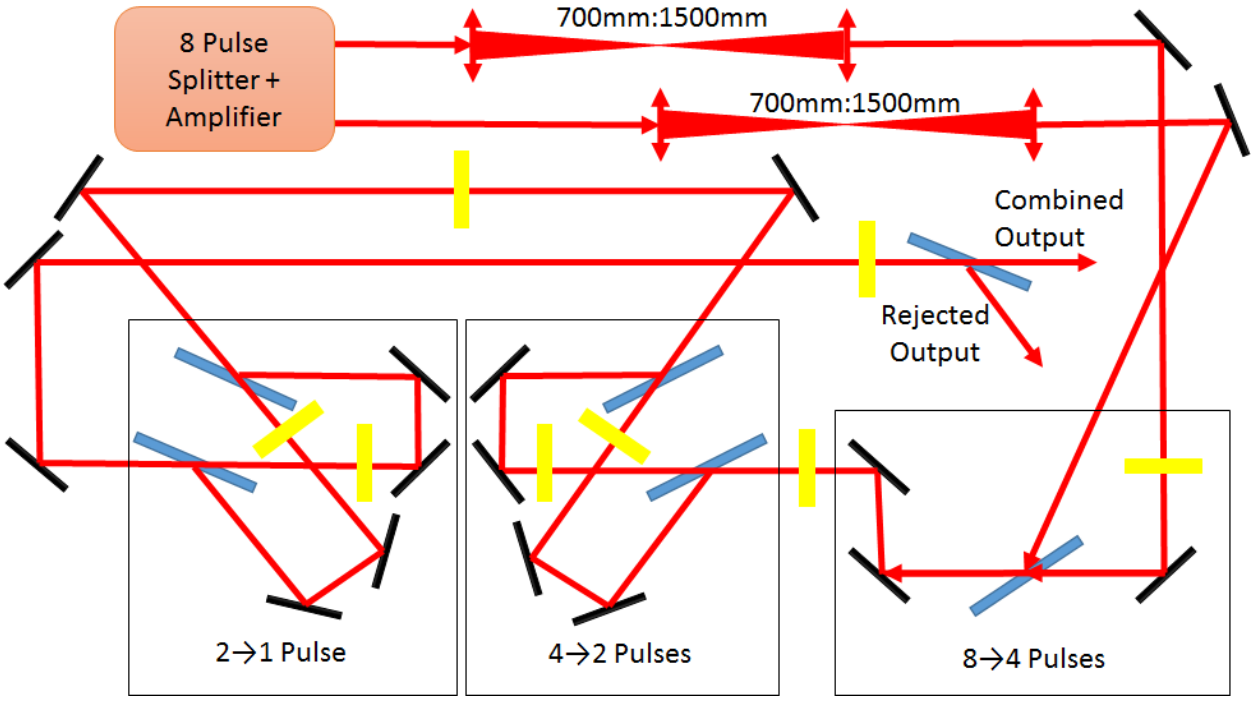

Figure 32: Schematic of the cascaded large-aperture 8 pulse combiner.

All pulses in the 8 pulse amplification stage see the same phase and amplitude noise which is generated during the flashlamp-pumping of the Nd:YAG rods. Therefore for a large number of pulse replicas, robust phase-locking can be achieved by passively phasing the pulses during amplification. This design contains the same benefits of the hybrid DPA scheme but also allows for the use of QWPs for circular polarization amplification. Thermalization effects which could arise in the case of high saturation could also be compensated by the introduced separation between the four amplifiers with relay imaging.

Cascaded combiners were designed for combining all 8 pulse replicas back into a single pulse (see figure 32). The spatial combiner first combines the spatially separated pulse replicas into 4 temporally divided pulses. Then two large-aperture combiners used in the hybrid configuration were used to combine the temporally divided pulses into a single output pulse. The mirrors and TFPs used in the combiner stage are all 3 inch in aperture since the beam is going to be imaged to 40 mm to avoid damaging the components.

CHAPTER 5: PHASE LOCKING

Obtaining mutual coherence between any number of pulses for CBC require that they be in phase. To ensure that there are no discrepancies in combination due to phase shifts from a multitude of sources, phase locking of the laser array is required [34]. Phase locking of a laser system is analogous to that in electronics where input signals are detected and through signal processing algorithms, an output error signal is sent to an active control element so that all phases are matched or locked [35]. However, locking of a laser signal requires a method for optical detection that generates electronic signals for processing. Laser locking schemes incorporate diagnostics of either individual beam elements or the combined/uncombined output beam to generate electronic signals for processing. The phase error signal for the phase locked loop is from the detected laser signal. Thus the performance of the PLL is highly dependent on quality of the sampled laser signal. In addition, there must be a relatively high signal-to-noise (SNR) ratio, especially in the presence of high amplitude (loud) noise sources. As will be discussed in further detail, for a flashlamp-pumped amplifier this may become a problem for slow feedback loops.

Hansch-Couillaud (HC) and LOCSET (Locking of Optical Coherence by Single-detector Electronic Tagging) are two common methods which provide phase locking through the use of photodetectors. The HC method is based upon elliptical polarization while the LOCSET method relies on beat interference for generating an error signal. Although the algorithm required to generate an error signal from an HC detector is much simpler than the LOCSET method, LOCSET requires only a single photodiode for analysis of phase error while HC requires a detector for every additional path length. Multiple detectors are needed for the use of HC in the locking of multiple beam elements. The only drawback of choosing the HC method over LOCSET would be the accumulation of a larger footprint.

Several elements can be placed in the optical path of the beamline to actively phase beam elements. Many active devices such as acousto-optic modulators and piezoelectric transducers have been widely used in many phase locking systems. Our active element of choice is the piezoelectric transducer (PZT) which when placed on a mirror can induce subwavelength path length correction [36]. PZT's are economical, easy to implement and reasonably small for use in large array systems. This chapter covers the operation of HC detectors, the development of electronics for phase locking, and the overall performance of our feedback system.

5.1 Active Phase Stabilization

The active phase stabilization system used in this thesis involves the use of the Hansch-Couillaud (HC) phase error detection scheme. A HC detector has three essential components which are required for measuring the phase error of a laser signal: a QWP, PBS and two photodiodes [37]. A laser which has mixed horizontal and vertical linear polarization components with a phase difference is transformed into an elliptical polarization. The instantaneous amplitudes of the horizontal and vertical electric field intensities are also dependent upon the elliptical orientation. The general mathematical description of elliptically polarized light is by

$$\left(\frac{\widetilde{E_x}}{E_{x0}}\right)^2 - 2\cos(\Delta\varphi)\left(\frac{\widetilde{E_x}}{E_{x0}}\right)\left(\frac{\widetilde{E_y}}{E_{y0}}\right) + \left(\frac{\widetilde{E_y}}{E_{y0}}\right)^2 = \sin^2\Delta\varphi \qquad (5.1)$$

where $\widetilde{E_x}/\widetilde{E_y}$ and E_{x0}/E_{y0} are the instantaneous and peak electric field intensity of the horizontal/vertical polarization components. A QWP can be used to transform the elliptical polarization into two orthogonal linear polarization components with an amplitude difference dependent upon the phase difference. A PBS can then be used to resolve the instantaneous electric field intensities of the two polarization components and measure the phase difference by placing a photodiode at each arm of the PBS. The incident light at both photodiodes will generate a current

proportional to the amplitude of the polarization component. This outlines the basic process in which the phase error accumulation of the laser can be measured using polarization. For our system, the p-polarized path of the splitter is taken as the reference, where the s-polarized component will be locked to the p-polarized path.

The difference of the two currents generated from the photodiodes is then used an error signal. This can be done using a differential amplifier or by subtracting the values through a microprocessor. A mathematical expression of the signal determined after taking the difference is given in by

$$HC - signal = \sqrt{I_1 I_2}\sin(\Delta\varphi) \qquad (5.2)$$

where I_1 and I_2 are the intensities incident on the two photodiodes and $\Delta\varphi$ is the phase difference between the two arms. The value of $\Delta\varphi$, which changes over time with the input signals, can be calculated directly by

$$\Delta\varphi = sin^{-1}\left(\frac{I_2 - I_1}{\sqrt{I_1 I_2}}\right). \qquad (5.3)$$

Equation 5.3 can be used to calculate the phase error continuously using a microprocessor with sufficient memory to perform the calculation from the input photocurrents.

Two phase locking circuits were developed, one called the Arduino circuit while the other called the Duck circuit (see figure 33). The Arduino circuit was built using a breadboard, an Arduino Mega microcontroller and a LabVIEW software programmed by Michael Chini was used to interface the circuit. The Duck circuit was built by Nathan Bodnar using custom electronics and software. The differences between the two circuits included different clock speeds of the microprocessors, acquisition loop times of the phase error and different software interfaces. In addition, the Duck circuit included a trigger feature which could select when to sample data and when to ignore data such as when the lamps fire in the amplifiers.

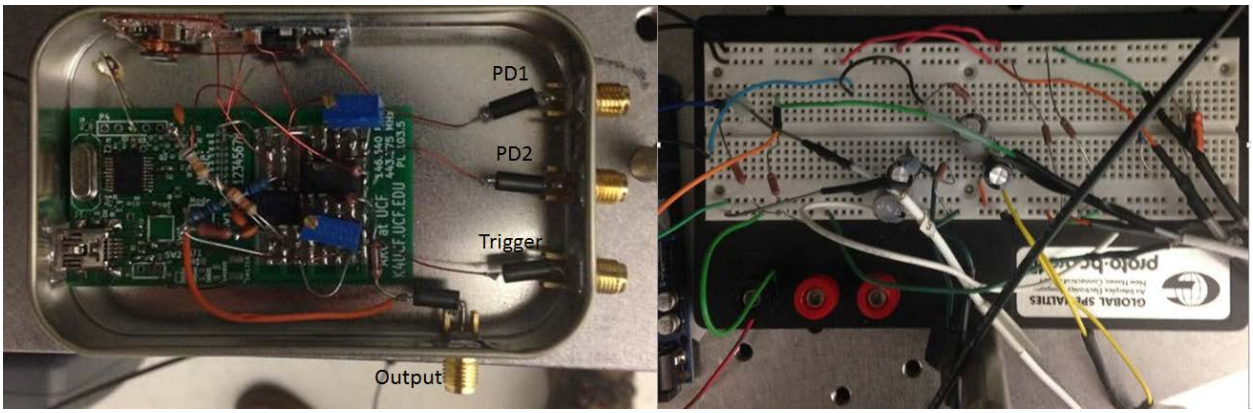

Figure 33: Left: Duck circuit. Right: Arduino circuit.

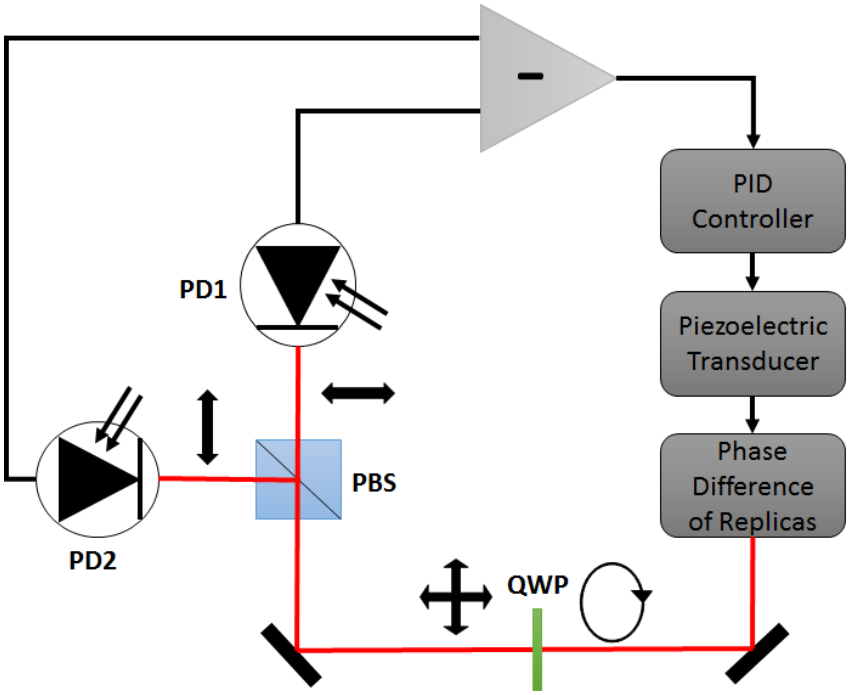

Figure 34: Diagram of the Hansch-Couillaud phase locking scheme.

Both circuits analyze the photocurrent generated by the photodiodes from the HC detector (figure 34) using a proportional-integral-differential (PID) algorithm where the proportional, integral and differential parameters scale the output error signal differently. The PID algorithm [35] is an effective feedback mechanism for the control of many closed-loop control systems.

$$u(t) = Pe(t) + I\int_0^t e(\tau)d\tau + D\frac{d}{dt}e(t) \qquad (5.4)$$

The proportional (P) parameter is to suppress error of the current processed signal, the integral (I) parameter is used to account for the error of previously processed values and lastly the differential (D) parameter is used to determine possible error values based on the rate of change of the current signal. In our algorithm we only established P and I parameters which were sufficient enough to lock the phase of the splitter.

From the PID algorithm, an output voltage signal can now be produced to drive the PZT placed on the end mirror of the splitter. The operation of the PZT relies on the piezoelectric effect which creates expansion of a material when applied to a voltage [36]. Thus by varying the voltage signal using a pulse-width modulation (PWM) signal generated by the PID and error signal, a feedback loop is now created by modulating the PZT. The movement of the PZT is on the order of a micron and thus can make fine adjustments of the optical path length by moving the mirror which it is mounted on. Thus through the feedback the stabilization of the two paths of the interferometer can be done with subwavelength precision, a criteria required for effective phase locking of a laser signal [38]. Since the pulses in the system operate at 2.5 Hz, a secondary CW pilot laser was needed for providing a feedback sampling rate long enough to generate stable phase locking. This created complexity in the overall system since two beams had to be aligned through a series of amplifiers and optical systems, however it was accomplished.

5.2 Passive Noise Suppression

In an effort to maximally reduce the coupling of noise with the laser system, several things can be done to suppress noise passively. For a large footprint system, the existence of noise can come from the laser itself. One example of this was the pulsing of the water in our chilled water lines running through the 19 mm amplifier modules. The pulsing was caused by the vibrations from the high-voltage flashlamps. It was difficult to initiate active phase locking while the pulsing

in the chilled water hosing was touching the optical table. After propping the hosing up such that it did not come into contact with the table, phase locking starts immediately and ran smoothly in the steady-state.

In the laser system used in this thesis, several optical tables were used to perform the experiments. The tables were placed tightly side-by-side, however they are still not interconnected. Thus each table can experience slightly varying vibrations which can be harmful for the performance of the PLL. In an effort to suppress the variations of the vibrations across each optical table metal braces were used to connect each table. By placing four braces in the interface between two tables and tightly screwing them in, this allows an interconnection between all the tables and thus dampens the noise fluctuation between them.

Using a MI with a Helium-Neon (HeNe) CW laser measurements of the stability and noise suppression of the braces were quantified. First a power spectral density (PSD) plot (figure 35) was constructed to analyze the noise frequency noise stabilized by the braces. Noise frequencies on the order of a few Hertz and below were stabilized passively.

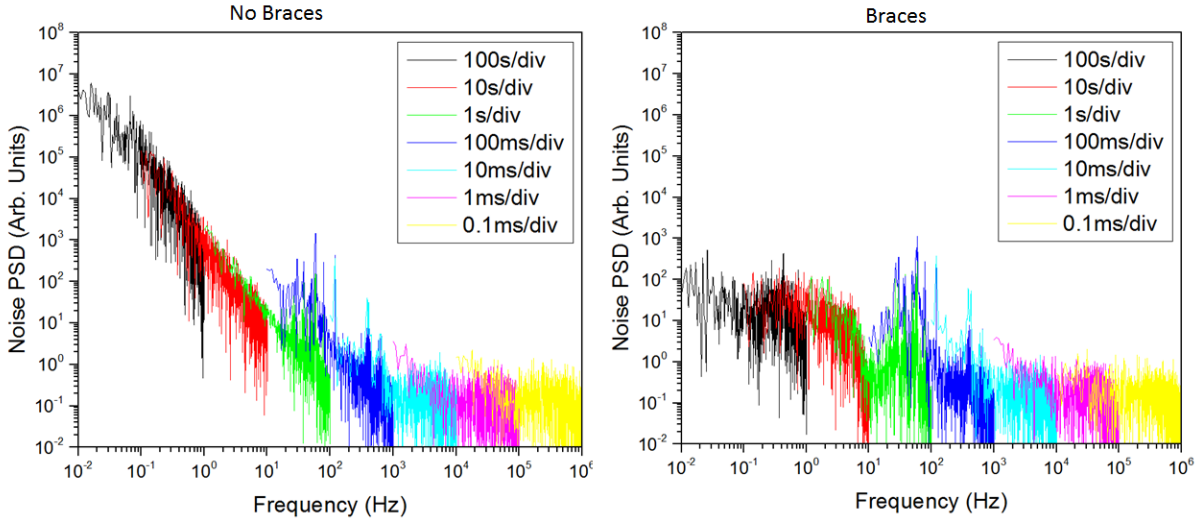

Figure 35: Left: Noise power spectral density with the interferometer free running (braces loosened). Right: Noise power spectral density with braces tightly locked.

Then an analysis of the stability of the braces on the optical table was made by introducing several fringes in the output of the MI. By slight misalignment on one of the arms of the interferometer, several fringes can be made shown in figure 36. By hitting the table five times, it was seen that the braces had a much faster response time to returning to the original fringe.

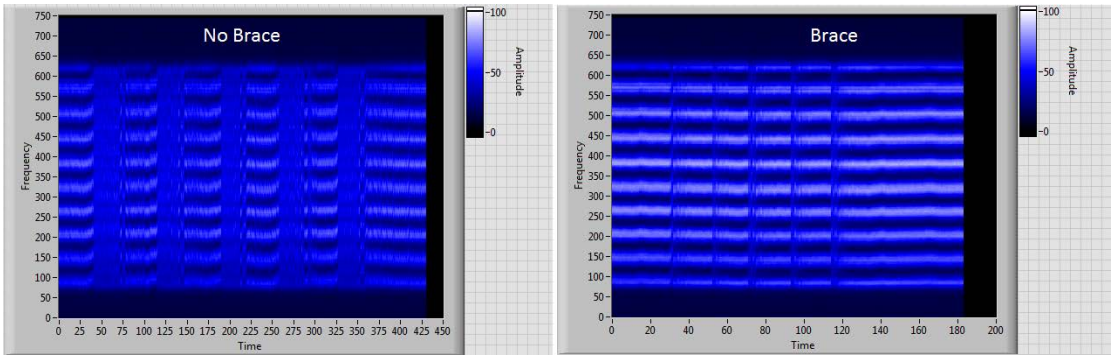

Figure 36: Left: Fringe visibility and response to hitting the table 5 times with no braces. Right: Fringe visibility and response to hitting the table 5 times with the braces.

The braces were perhaps the only modifications to the facility which showed significant improvement in the reduction of the noise floor. Other existing noise sources in the laboratory include fans, noisy equipment from neighboring laboratories and large chillers in the chase way. An enclosure was also built around the optical table to keep the facility clean for high-power operation as well as preventing turbulent air flow across the table. These factors may be minor in the performance of the locking which can be further improved through improvement of the PLL itself.

5.3 Performance of Steady-State Operation

The performance of the phase locking used in the active DPA experiments was robust for the single channel experiments. Figure 37 shows the difference of the CW and pulsed beams while free running and locked. Both beams were locked with a phase error less than 250 mrad over long periods of time. The operation of the locking ran almost continuously under the condition that

none of the amplifiers were on. In the case where the 19 mm amplifiers were on and pumped at max voltage, the locking would operate for about 10-15 minutes before the locking was lost due to drifts of the output voltage. Controlling the output voltage signal by changing PID parameters helped stabilize the circuit longer for certain conditions.

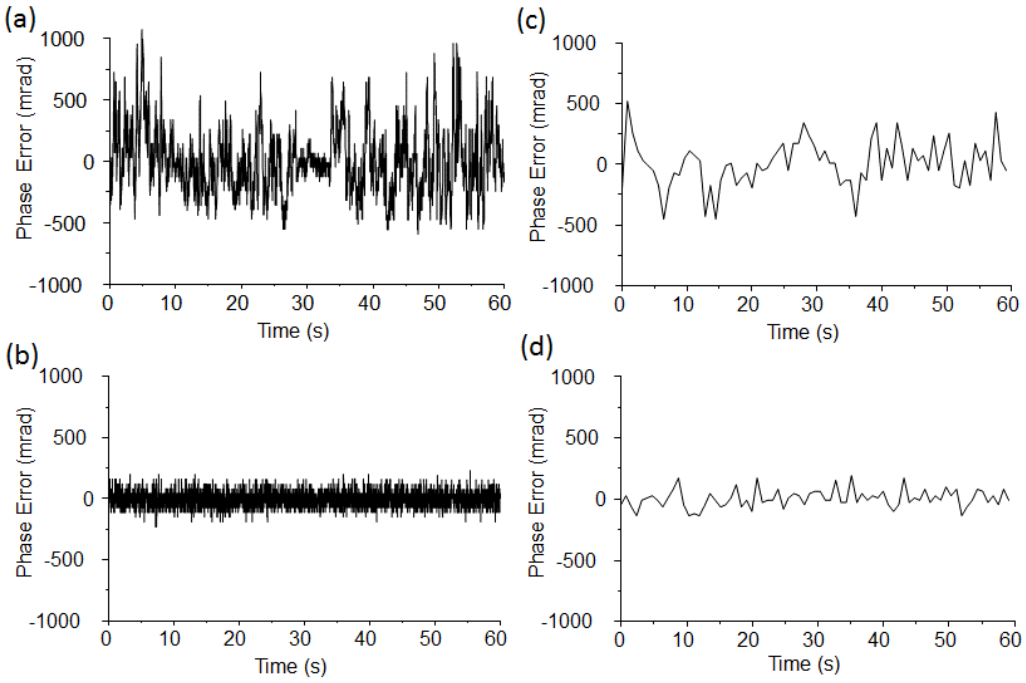

Figure 37: (a) CW free running phase error. (b) CW locked phase error. (c) Pulsed free running phase error. (d) Pulsed locked phase error.

The root-mean-square (RMS) phase error calculated from these results were 58 mrad and 90 mrad for the CW and pulsed beams respectively. In the pulsed beam, the corresponding intensity variation was 0.4%, showing a highly stable output from the output of system. A PSD plot comparing the unlocked and locked cases were made to characterize the frequency ranges which were suppressed by the PLL. It was found that frequencies below 2 Hz were most effectively suppressed by both circuits (figure 38).

In a comparison of the Duck circuit versus the Arduino circuit, they came close to suppressing the same level of noise, both in the sub-2 Hz range. From the PSD plot comparing the

circuits in figure 38 it appears that the Arduino circuit had slightly suppressed more noise than the Duck circuit. Although the two PSD plots were taken quickly after one another measurement errors could have affected the outcome of the data. The sudden reduction of some low frequencies in between measurements could have created this amplitude difference but overall the two circuits seem equal.

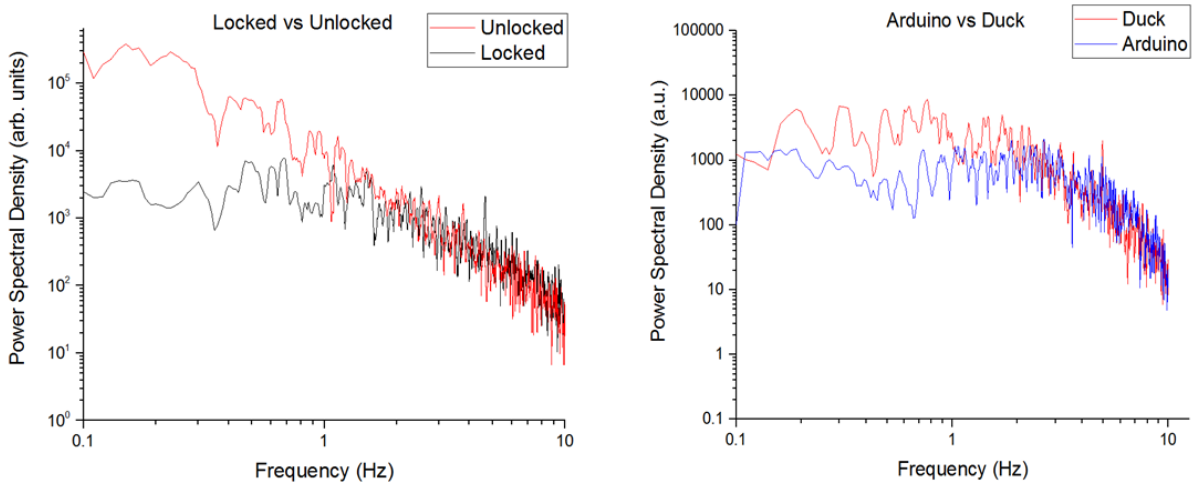

Figure 38: Left: Noise PSD of the locked/unlocked CW laser. Right: Noise PSD of the locked CW laser using either the Duck or Arduino circuit.

CHAPTER 6: CONCLUSION

In this thesis I have presented the coherent combination of picosecond pulses in active, passive and hybrid configurations. A record combining energy (216 mJ) has been achieved using the method of DPA in a Nd:YAG laser. The hybrid DPA technique, to the best of our knowledge, has been demonstrated for the first time. In addition, robust indirect phase locking of a DPA-based laser system using a CW pilot laser has also been demonstrated.

CBC will allow many fields in the physical sciences to flourish by providing next generation lasers. Theoretical and experimental improvements to CBC are certain to continue in the future. The following are applications that can be benefited from the development of CBC.

6.1 Attosecond Science

Using intense few-cycle pulses, the first ever attosecond pulses were generated from an electron re-colliding with its parent ion [39]. With the development of the high-order harmonic generation model, attosecond pulses were soon realized using high-power femtosecond driving lasers. Generation of pulses in this time regime have given resolution of electronic and atomic processes almost approaching the fundamental unit of time which is about 24 attoseconds. Thus further development of attosecond technology will lead to fundamental understanding of not only dynamics of the quantum realm but also control of these processes for applications such as communications [40].

High-order harmonic generation, similar to second and third harmonic generation, is strictly tied to nonlinear optical processes which occur with high-intensity laser fields. The method has been demonstrated in various schemes that can all be described by the three-step model. The three-step model outlines the physical processes which takes place between an incident

femtosecond driving laser and a target, usually noble gases or solid targets. The three processes which occur are ionization, acceleration and recombination.

In the first step of the model, a strong few- or single-cycle femtosecond laser field is focused into a target that is within the Rayleigh range for ionization. Then in the second stage, an electron that is ionized will be accelerated by the electric field of the laser. The electron accelerates towards the direction of field, thus as the laser field reaches its peak and switches directions the electron now accelerates back and eventually collides with the parent ion emitting a photon. Several electrons can be ionized from an atom, generating a free electron pulse during the ionization process. Thus the coherent superposition of the emitted photons from the electron pulse will give the rise to an attosecond pulse much shorter than the femtosecond driving laser [11].

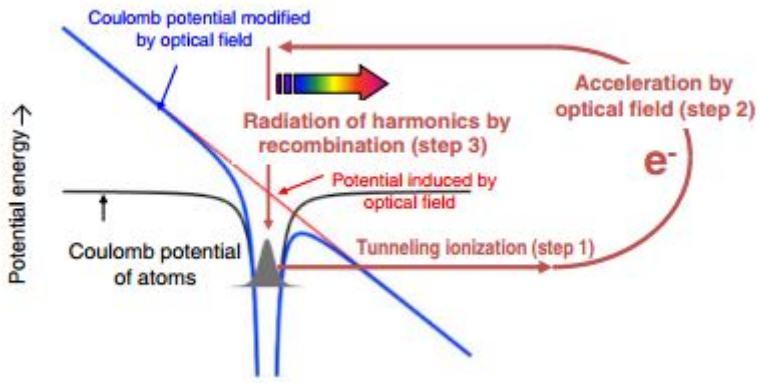

Figure 39: Three step model of high-order harmonic generation. From [39].

In recent discoveries, isolated attosecond pulses (IAP) have been used to measure electron dynamics. Transient attosecond spectroscopy has provided insight into the evolution of ionization, absorption and quantum interference in selected electronic states of atoms [40]. Limitations on peak power of these IAP's have withheld its true potential for characterization of dynamics in complex structures [41]. With the development of coherently synthesized ultrabroadband attosecond pulses, electric fields can be well shaped to appropriately probe selected materials since

for ionization experiments, it is unwise to apply a field with intensities larger than the threshold in order to preserve atomic resonances [6].

6.2 Laser Fusion

Many large footprint laser facilities have been built and are currently under construction for inertial confinement fusion (ICF) experiments. Notable facilities include the National Ignition Facility (NIF) [42], the OMEGA laser at the Laboratory of Laser Energetics [43] and Laser MegaJoule [44]. Bombardment of ultra-intense pulses on fuel pellets to induce implosion is necessary for fusion [42]. These laser facilities aim for both high-energy and high-peak power in multiple single-beamline architectures. Nonlinear frequency conversion is usually done in each beamline before being sent to the target. In the target chamber, each beamline is tightly focused and phased such that they arrive with ultra-high-intensity at the small target usually held inside a hohlraum [45]. The current challenges in achieving successful fusion is obtaining a higher energy output from the interaction than the total amount of energy used for operation of the facility, including not only the energy of laser input but also the power consumption of the facility. Currently, the intensities which are delivered to the target chamber are from multiple beamlines. If the DPA technique was utilized for each beamline using femtosecond pulses, the current intensities of these facilities can be greatly increased. Utilizing CBC in the development of diode-pumped solid-state lasers may be the key for achieving ignition [46]. CBC can be a gateway to achieving compact fusion reactors with beyond petawatt peak powers, high repetition rates and excellent beam quality.

LIST OF REFERENCES

1] W. T. Silfvast, *Laser Fundamentals*. Cambridge University Press, 2004.

[2] J.-C. Diels and W. Rudolph, *Ultrashort Laser Pulse Phenomena: Fundamentals, Techniques, and Applications on a Femtosecond Time Scale*. Academic Press, 2006.

[3] G. New, *Introduction to Nonlinear Optics*. Cambridge University Press, 2011.

[4] M. Scheller, M. S. Mills, M.-A. Miri, W. Cheng, J. V. Moloney, M. Kolesik, P. Polynkin, and D. N. Christodoulides, "Externally refuelled optical filaments," *Nat. Photonics*, vol. 8, no. 4, pp. 297–301, Mar. 2014.

[5] A. Hunter, R. Hunter, and T. Johnson, "Scaling of KrF lasers for inertial confinement fusion," *IEEE J. Quantum Electron.*, vol. 22, no. 3, pp. 386–404, Mar. 1986.

[6] Y. Wu, E. Cunningham, H. Zang, J. Li, M. Chini, X. Wang, Y. Wang, K. Zhao, and Z. Chang, "Generation of high-flux attosecond extreme ultraviolet continuum with a 10 TW laser," *Appl. Phys. Lett.*, vol. 102, no. 20, p. 201104, May 2013.

[7] H. Kiriyama, T. Shimomura, H. Sasao, Y. Nakai, M. Tanoue, S. Kondo, S. Kanazawa, A. S. Pirozhkov, M. Mori, Y. Fukuda, M. Nishiuchi, M. Kando, S. V. Bulanov, K. Nagashima, M. Yamagiwa, K. Kondo, A. Sugiyama, P. R. Bolton, T. Tajima, and N. Miyanaga, "Temporal contrast enhancement of petawatt-class laser pulses," *Opt. Lett.*, vol. 37, no. 16, p. 3363, 2012.

[8] D. Strickland and G. Mourou, "Compression of amplified chirped optical pulses," *Opt. Commun.*, vol. 55, no. 6, pp. 447–449, Oct. 1985.

[9] E. S. Lamb, L. G. Wright, and F. W. Wise, "Divided-pulse lasers.," *Opt. Lett.*, vol. 39, no. 9, pp. 2775–7, 2014.

[10] J. Zhou, G. Taft, C.-P. Huang, M. M. Murnane, H. C. Kapteyn, and I. P. Christov, "Pulse evolution in a broad-bandwidth Ti:sapphire laser," *Opt. Lett.*, vol. 19, no. 15, p. 1149, Aug. 1994.

[11] Z. Chang, *Fundamentals of Attosecond Optics*. CRC Press, 2011.

[12] S. Kane and J. Squier, "Fourth-order-dispersion limitations of aberration-free chirped-pulse amplification systems," *J. Opt. Soc. Am. B*, vol. 14, no. 5, p. 1237, May 1997.

[13] M. Pessot, J. Squier, G. Mourou, and D. J. Harter, "Chirped-pulse amplification of 100-fsec pulses," *Opt. Lett.*, vol. 14, no. 15, p. 797, Aug. 1989.

[14] Z. Wei, H. Han, W. Zhang, Y. Zhao, and J. Zhu, "Measurement and Control of Carrier-Envelope Phase in Femtosecond Ti : sapphire Laser," no. February, 2010.

[15] “Encyclopedia of Laser Physics and Technology - Carrier-envelope offset, CEO frequency, CEP, absolute phase.” [Online]. Available: https://www.rp-photonics.com/carrier_envelope_offset.html. [Accessed: 21-Apr-2016].

[16] K. Sala, M. Richardson, and N. Isenor, “Passive mode locking of lasers with the optical Kerr effect modulator,” *IEEE J. Quantum Electron.*, vol. 13, no. 11, pp. 915–924, Nov. 1977.

[17] M. Kienel, A. Klenke, T. Eidam, M. Baumgartl, C. Jauregui, J. Limpert, and A. Tünnermann, “Analysis of passively combined divided-pulse amplification as an energy-scaling concept,” *Opt. Express*, vol. 21, no. 23, pp. 29031–29042, 2013.

[18] A. Vaupel, N. Bodnar, B. Webb, L. Shah, and M. Richardson, “Concepts, performance review, and prospects of table-top, few-cycle optical parametric chirped-pulse amplification,” *Opt. Eng.*, vol. 53, no. 5, p. 051507, 2013.

[19] W. Koechner, *Solid-State Laser Engineering*. Springer Science & Business Media, 2006.

[20] A. E. Siegman, “Nonlinear Optical Effects: An Optical Power Limiter,” *Appl. Opt.*, vol. 1, no. 6, p. 739, Nov. 1962.

[21] J. Y. Zhang, J. Y. Huang, Y. R. Shen, and C. Chen, “Optical parametric generation and amplification in barium borate and lithium triborate crystals,” *J. Opt. Soc. Am. B*, vol. 10, no. 9, p. 1758, Sep. 1993.

[22] T. Kobayashi and A. Baltuska, “Sub-5 fs pulse generation from a noncollinear optical parametric amplifier,” *Meas. Sci. Technol.*, vol. 13, no. 11, pp. 1671–1682, Nov. 2002.

[23] G. Cerullo and S. De Silvestri, “Ultrafast optical parametric amplifiers,” *Rev. Sci. Instrum.*, vol. 74, no. 1, p. 1, Jan. 2003.

[24] A. Harth, M. Schultze, T. Lang, T. Binhammer, S. Rausch, and U. Morgner, “Two-color pumped OPCPA system emitting spectra spanning 1.5 octaves from VIS to NIR.,” *Opt. Express*, vol. 20, no. 3, pp. 3076–81, Jan. 2012.

[25] “RP Photonics Consulting GmbH - technical consulting on laser technology, nonlinear optics, fiber optics; simulation and design software; encyclopedia and buyer’s guide.” [Online]. Available: https://www.rp-photonics.com/. [Accessed: 23-Mar-2016].

[26] S. Zhou, D. G. Ouzounov, and F. W. Wise, “Divided-pulse amplification of ultrashort pulses,” *Conf. Lasers Electro-Optics, 2007, CLEO 2007*, vol. 32, no. 7, pp. 871–873, 2007.

[27] J. Limpert, A. Klenke, M. Kienel, S. Breitkopf, T. Eidam, S. Hadrich, C. Jauregui, and A. Tunnermann, “Performance Scaling of Ultrafast Laser Systems by Coherent Addition of Femtosecond Pulses,” *IEEE J. Sel. Top. Quantum Electron.*, vol. 20, no. 5, pp. 1–10,

2014.

[28] H. E. Bates, “Coherent birefringent optical pulse compression,” *J. Opt. Soc. Am.*, vol. 70, no. 8, p. 1017, 1980.

[29] M. Kienel, A. Klenke, T. Eidam, S. Hädrich, J. Limpert, and A. Tünnermann, “Energy scaling of femtosecond amplifiers using actively controlled divided-pulse amplification.,” *Opt. Lett.*, vol. 39, no. 4, pp. 1049–52, 2014.

[30] A. Klenke, M. Kienel, T. Eidam, S. Hädrich, J. Limpert, and A. Tünnermann, “Divided-pulse nonlinear compression.,” *Opt. Lett.*, vol. 38, no. 22, pp. 4593–6, 2013.

[31] Y. Zaouter, F. Guichard, L. Daniault, M. Hanna, F. Morin, C. Hönninger, E. Mottay, F. Druon, and P. Georges, “Femtosecond fiber chirped- and divided-pulse amplification system,” vol. 38, no. 2, pp. 106–108, 2013.

[32] L. Daniault, M. Hanna, D. N. Papadopoulos, Y. Zaouter, E. Mottay, F. Druon, and P. Georges, “High peak-power stretcher-free femtosecond fiber amplifier using passive spatio-temporal coherent combining,” *Opt. Express*, vol. 20, no. 19, p. 21627, 2012.

[33] D. N. Schimpf, T. Eidam, E. Seise, S. Hädrich, J. Limpert, and A. Tünnermann, “Circular versus linear polarization in laser-amplifiers with Kerr-nonlinearity.,” *Opt. Express*, vol. 17, no. 21, pp. 18774–18781, 2009.

[34] E. C. Cheung, J. G. Ho, G. D. Goodno, R. R. Rice, J. Rothenberg, P. Thielen, M. Weber, and M. Wickham, “Diffractive-optics-based beam combination of a phase-locked fiber laser array.,” *Opt. Lett.*, vol. 33, no. 4, pp. 354–356, 2008.

[35] M. A. Johnson and M. H. Moradi, Eds., *PID Control*. London: Springer-Verlag, 2005.

[36] R. Resmi and M. R. Baiju, “Performance analysis of a tunable piezoelectric actuator based MEMS resonator.” pp. 173–178, 2012.

[37] T. W. Hansch and B. Couillaud, “Laser Frequency Stabilization By Polarization Spectroscopy of a Reflecting Reference Cavity.,” *Opt. Commun.*, vol. 35, no. 3, pp. 441–444, 1980.

[38] *Coherent Laser Beam Combining*, vol. 13. Wiley, 2013.

[39] K. Midorikawa, “High-Order Harmonic Generation and Attosecond Science,” *Jpn. J. Appl. Phys.*, vol. 50, no. 9, p. 090001, Sep. 2011.

[40] M. Chini, K. Zhao, and Z. Chang, “The generation, characterization and applications of broadband isolated attosecond pulses,” *Nat. Photonics*, vol. 8, no. 3, pp. 178–186, Feb. 2014.

[41] M. Chini, X. Wang, Y. Cheng, H. Wang, Y. Wu, E. Cunningham, P.-C. Li, J. Heslar, D.

A. Telnov, S.-I. Chu, and Z. Chang, “Coherent phase-matched VUV generation by field-controlled bound states,” *Nat. Photonics*, vol. 8, no. 6, pp. 437–441, May 2014.

[42] O. A. Hurricane, D. A. Callahan, D. T. Casey, P. M. Celliers, C. Cerjan, E. L. Dewald, T. R. Dittrich, T. Döppner, D. E. Hinkel, L. F. Berzak Hopkins, J. L. Kline, S. Le Pape, T. Ma, A. G. MacPhee, J. L. Milovich, A. Pak, H.-S. Park, P. K. Patel, B. A. Remington, J. D. Salmonson, P. T. Springer, and R. Tommasini, “Fuel gain exceeding unity in an inertially confined fusion implosion.,” *Nature*, vol. 506, no. 7488, pp. 343–8, Feb. 2014.

[43] “LLE Review.” [Online]. Available: http://www.lle.rochester.edu/media/publications/lle_review/documents/v144/144_Review.pdf. [Accessed: 23-Mar-2016].

[44] “THE LASER MEGAJOULE FACILITY: CONTROL SYSTEM STATUS REPORT.” [Online]. Available: https://accelconf.web.cern.ch/accelconf/ica07/PAPERS/MOAB02.PDF. [Accessed: 23-Mar-2016].

[45] D. M. Pennington, C. G. Brown, T. E. Cowan, S. P. Hatchett, E. Henry, S. Herman, M. Kartz, M. Key, J. Koch, A. J. MacKinnon, M. D. Perry, T. W. Phillips, M. Roth, T. C. Sangster, M. Singh, R. A. Snavely, M. Stoyer, B. C. Stuart, and S. C. Wilks, “Petawatt laser system and experiments,” *IEEE J. Sel. Top. Quantum Electron.*, vol. 6, no. 4, pp. 676–688, Jul. 2000.

[46] S. Nakai, M. Nakatsuka, M. Yamanaka, Y. Kozaki, N. Miyanaga, E. Yoshida, K. Tsubakimoto, H. Kiriyama, H. Matsui, H. Azechi, H. Takabe, T. Yamanaka, K. Mima, and H. P. K. K, “Development of diode pumped solid state laser and its application to laser fusion and industry,” vol. 3343, no. April 1998.